Master's thesis

Environmental Technology

2019

Heikki Kauppi

PHYSICAL PROPERTIES AND SOLUBILITY PROPERTIES OF TRIMETHYLGLYCINE-BASED DEEP EUTECTIC SOLVENTS

TURKU AMK
TURKU UNIVERSITY OF APPLIED SCIENCES

MASTER'S THESIS | ABSTRACT

TURKU UNIVERSITY OF APPLIED SCIENCES

Environmental Technology

2019 | 72 pages

Heikki Kauppi

PHYSICAL PROPERTIES AND SOLUBILITY PROPERTIES OF TRIMETHYLGLYCINE-BASED DEEP EUTECTIC SOLVENTS

The purpose of this thesis was to create an information source for the employer containing an overview of biomass properties, and a summary to ionic liquids and deep eutectic solvents. The gathered information was then used to study the physicochemical properties of six deep eutectic solvents and their ability to dissolve lignosulfonate.

In the literature section information was summed up of a composition of biomass, its structure, and chemical properties, additionally, lignosulfonates were studied in this section. Ionic liquids and deep eutectic solvents were studied in more detail in the second part of biomass pretreatment methods.

Six deep eutectic solvents were studies in the experimental section, two of them were immediately discarded from further testing. Viscosity and conductivity were measured in different temperatures from these solvents. A Walden plot was created from these results, the relative strength of ionicity was defined from this plot. Two lignosulfonate-based sediments were studies with various analysis methods and finally, the deep eutectic solvent's ability to dissolve the sediments was measured.

This study showed that urea, acetic acid, lactic acid, and formic acid formed a eutectic solvent with betaine. The viscosity of these solvents was measured, and it decreased in the following order: lactic acid > acetic acid > urea > formic acid. Conductivity followed the following order: formic acid > lactic acid > acetic acid > urea. A Walden plot was created from these results and the order of ionicity decreased in the following order: formic acid > lactic acid > acetic acid > urea. Solvents' ability to dissolve lignosulfonate was determined by spectrophotometric. Urea-based solvent dissolved the sample completely and formic acid-based the least. Surprisingly ionicity was noticed to correlate with the dissolving ability very strongly (correlation factor R^2=0,9904). One of the sediments, furfural coal, was noticed to dissolve easily in mild 0,1M NaOH solution, so its dissolution was not studied with the deep eutectic solvents. The molar mass of furfural coal was determined to be on average ca. 750 g/mol.

KEYWORDS:

biomass, lignin, ionic liquid, deep eutectic solvent, betaine

OPINNÄYTETYÖ (YAMK) | TIIVISTELMÄ

TURUN AMMATTIKORKEAKOULU

Ympäristötekniikan koulutusohjelma

2019 | 72 sivua

Heikki Kauppi

TRIMETYYLIGLYSIINI-POHJAISTEN SYVÄEUTEKTISTEN SEOSTEN FYSIKAALISET OMINAISUUDET JA LIUOTUSOMINAISUUDET

Työn tarkoituksena oli luoda tietolähde työnantajalle sisältäen katsauksen biomassan ominaisuuksiin, sekä yhteenveto ionisiin nesteihin ja eutektisiin seoksiin. Lisäksi työssä käytettiin em. tietoja hyväksi tutkittaessa kuuden betaiinipohjaisen eutektisen seoksen fysikaalisia ominaisuuksia ja niiden kykyä liuottaa lignosulfonaattisakkaa.

Kirjallisuusosassa perehdyttiin biomassan eri komponentteihin, niiden rakenteeseen ja kemiallisiin ominaisuuksiin, lisäksi tehtiin katsaus lignosulfonaatteihin. Biomassan esikäsittelymenetelmistä käsiteltiin tarkemmin ionisia nesteitä ja eutektisiä seoksia. Niiden fysikaalisia ominaisuuksia, rakennetta ja käyttöä käytiin läpi.

Kokeellisessa osassa tutkittiin kuutta eri eutektista seosta, joista kaksi hylättiin heti alussa. Seoksista määritettiin viskositeetti ja johtokyky eri lämpötiloissa, tuloksista piirrettiin Waldenin graafi, jolla määritettiin seosten keskinäinen ionisuuden voimakkuus. Kahta lignosulfonaattipohjaista sakkaa tutkittiin eri analyysimenetelmillä ja lopuksi määritettiin neljän eutektisen seoksen kyky liuottaa näitä sakkoja.

Työssä osoitettiin, että urea, etikkahappo, maitohappo ja muurahaishappo muodostivat eutektinen seoksen betaiinin kanssa. Näille seoksille määritettiin viskositeetti, seosten järjestys korkeimmasta matalimpaan oli: maitohappo > etikkahappo > urea > muurahaishappo. Seosten johtokyky oli järjestyksessä korkeimmasta matalimpaan: muurahaishappo > maitohappo > etikkahappo > urea. Waldenin graafista määritettiin seosten ionisuuden voimakkuuden olevan korkeimmasta matalimpaan: muurahaishappo > maitohappo > etikkahappo > urea. Seosten kyky liuottaa lignosulfonaattisakkaa määritettiin spektrofotometrisesti, ureapohjainen seos liuotti näytteen kokonaisuudessaan ja muurahaishappopohjainen seos heikoiten. Yllättävästi ionisuuden voimakkuuden todettiin korreloivan sakan liuotuspotentiaalin kanssa erittäin hyvin (korrelaatiokerroin R^2=0,9904). Toisen sakoista, furfuraalihiilen, todettiin liukenevan erittäin helposti laimeaan 0,1M NaOH liuokseen, joten sen liukoisuutta eutektisiin seoksiin ei tutkittu. Furfuraalihiilen moolimassaksi mitattiin keskimäärin n. 750 g/mol.

ASIASANAT:

biomassa, ligniini, ioninen neste, eutektinen seos, betaiini

CONTENT

LIST OF ABBREVIATIONS (OR) SYMBOLS **8**

1 INTRODUCTION **10**

2 LIGNOCELLULOSIC BIOMASS **11**

2.1 Softwood biomass 11

2.2 Hardwood biomass 12

2.3 Grass and energy crop biomass 13

2.4 Agricultural residue 13

3 COMPOSITION OF LIGNOCELLULOSIC BIOMASS **15**

3.1 Cellulose 15

3.2 Hemicelluloses 16

3.2.1 Softwood hemicellulose 17

3.2.2 Hardwood hemicellulose 19

3.2.3 Grass and agricultural residue hemicellulose 19

3.3 Lignin 20

3.3.1 Chemical structure 21

3.3.2 Lignin-carbohydrate complex 22

3.3.3 Molecule weight 23

3.3.4 Dispersity index 23

3.3.5 Solubility 25

3.3.6 Chemical classification 25

3.3.7 Model compounds of native lignin 28

4 LIGNOSULFONATES **30**

5 PRETREATMENT METHODS **32**

5.1 Ionic liquids 33

5.2 Deep eutectic solvents 34

5.2.1 Composition 35

5.2.2 The melting point and phase diagram 36

5.3 Natural deep eutectic solvents 38

5.4 Low transition temperature mixtures 38

5.5 Chemical properties 39

5.5.1 Viscosity 39
5.5.2 Conductivity 40
5.5.3 Density 41
5.5.4 Ionicity 42
5.5.5 Ultraviolet-visible spectroscopy 43

6 EXPERIMENTAL PART 44
6.1 Materials 44
6.2 Trimethylglycine 45
6.3 Analysis of the prepared DESs 45
6.3.1 Water content 46
6.3.2 Viscosity 46
6.3.3 Conductivity 48
6.3.4 Walden plot 50
6.3.5 UV-VIS spectroscopy 51
6.3.6 Distillation 52
6.4 Sediment sample analysis 53
6.4.1 Furfural coal 53
6.4.2 Lignosulfonate 58
6.5 The solubility of tested samples 59
6.5.1 Furfural coal sample 59
6.5.2 Lignosulfonate sample 59

7 CONCLUSION AND DISCUSSION 65
7.1 DES properties 65
7.2 Sediment properties 66
7.3 DES dissolution properties 66
7.4 A further point of interest 66

REFERENCES 67

FIGURES

Figure 1. Chemical structure of cellulose 15
Figure 2. A typical structure of galactoglucomannan 18
Figure 3. Structure of softwood arabinoglucuronoxylan 18
Figure 4. An example structure of arabinoxylan 20
Figure 5. Three lignin precursors 21
Figure 6. Common types of lignin linkage 27
Figure 7. Contemporary View of Lignin Substructures 28
Figure 8. Sulfonation reaction of lignin in acid sulfite pulping 31
Figure 9. Standard DES components 35
Figure 10. Example of the eutectic phase diagram of components A and B 37
Figure 11. An arbitrary example of different ionic liquids 42
Figure 12. Chemical structure of Trimethylglycine (A) and Choline Chloride (B) 45
Figure 13. Measured and modeled (VFT) viscosities in different temperatures 47
Figure 14. DESs conductivity at different temperatures 49
Figure 15. Walden plot of all four tested DES solutions 50
Figure 16. Background absorbance of tested DESs 52
Figure 17. Molecular weight distribution chromatogram of furfural coal 57
Figure 18. UV-VIS absorption curve of the lignosulfonate sample 60
Figure 19. Absorbance calibration curve of the lignosulfonate sample 61
Figure 20. Absorption curve of dissolved LS in different DESs 62
Figure 21. Correlation of ΔW and dissolved lignosulfonate 64

EQUATIONS

Equation 1. Dispersity index 23
Equation 2. The general formula for a deep eutectic solvent 34
Equation 3. The Arrhenius equation 39
Equation 4. The Litovitz equation 40
Equation 5. The Vogel-Fulcher-Tammann equation 40
Equation 6. Molar conductivity 41
Equation 7. A linear equation for density 41
Equation 8. Exponential second-order equation 41
Equation 9. Beer-Lambert law 43

PICTURES

Picture 1. Dried furfural coal. 54
Picture 2. Hardened furfural coal. 54
Picture 3. Lignosulfonate sample. 58
Picture 4. DES sample of the lignosulfonate dissolution test. 63

TABLES

Table 1. Typical composition of common softwoods 12
Table 2. Typical composition of common hardwoods 12
Table 3 Composition of common grasses and energy crops 13
Table 4. Average composition of different agricultural residues 14
Table 5. Summary of most common hemicelluloses 17
Table 6. Effect of isolation method on different softwood lignin 24
Table 7. M_n, M_w, and $Đ_M$ of two different lignin 24
Table 8. Distribution of lignin precursors from different lignin sources 26
Table 9. Distribution of linkage types in different lignin sources 26
Table 10. Sulfite pulping processes 30
Table 11. Overview of biomass pretreatment methods 33
Table 12. Reported eutectic composition of various DESs 36
Table 13. Prepared DESs, their molar ratios, and target water percentages 44
Table 14. The water content of the starting material and samples 46
Table 15. Measured and modeled viscosities of BE:UR 48
Table 16. Fitting parameters and RMSE of the VFT equation for viscosity 48
Table 17. Fitting parameters and RMSE of the VFT equation for conductivity 49
Table 18. Summary table of the DES background testing 51
Table 19. The dry substance of BE:UR feed and distillate 53
Table 20. Elemental composition of the furfural coal analyzed by Lenzing AG 55
Table 21. Elemental composition of the furfural coal 55
Table 22. HPLC analysis of furfural coal 56
Table 23. Estimated M_w distribution of furfural coal 57
Table 24. Solubility scan of FC at different pH 59
Table 25. A molar attenuation coefficient of the lignosulfonate sample 61
Table 26. Dissolved lignosulfonate 62

LIST OF ABBREVIATIONS (OR) SYMBOLS

AQ	Anthraquinone
AX	Arabinoxylan
AGX	Arabinoglucuronoxylan
CEL	Cellulolytic enzyme lignin
DES	Deep eutectic solvent
EMAL	Enzymatic mild acidolysis lignin
FC	Furfural coal
GGM	Galactoglucomannan
GM	Glucomannan
HBD	Hydrogen bond donor
HMF	Hydroxymethylfurfural
HPLC	High-performance liquid chromatography
IL	Ionic liquid
LCB	Lignocellulosic biomass
LCC	Lignin-carbohydrate complex
LMM	Low-melting mixture
LTTM	Low transition temperature mixture
LS	Lignosulfonate
MWL	Milled wood lignin
NADES	Natural deep eutectic solvent
NAMW	Number-average molar weight, g/mol

NaOH	Sodium hydroxide
NSSC	Neutral sulfite semi-chemical
TMG	Trimethylglycine
WAMW	Weight-average molar weight, g/mol

A	Constant
B	Constant
Da	Dalton, [$g \cdot mol^{-1}$]
$Đ_M$	Dispersity index
E_η	Activation energy, [$kJ \cdot mol^{-1}$]
M_n	Number-average molecular weight, [$g \cdot mol^{-1}$]
M_w	Weight-average molecular weight, [$g \cdot mol^{-1}$]
η	Viscosity, [mPas]
η_0	Constant
R	Universal gas constant, [$J \cdot K^{-1} \cdot mol^{-1}$]
T	Temperature, [°C or K]
T_0	Ideal glass temperature, [°C or K]
T_f	Freezing point, [°C or K]
T_g	Glass transition temperature, [°C or K]
T_m	Melting point, [°C or K]

1 INTRODUCTION

It has been long evident, that increasing demand for consumer goods cannot be satisfied with fossil-based materials and the need to decrease the carbon footprint of the society: these facts pave the road for new sustainable innovations. The investigation has been ongoing for decades to replace fossil-based materials with more environmentally friendly alternatives. In recent years significant breakthroughs have been achieved with lignocellulosic feedstock.

Reviewing the scientific references shows a great interest in lignocellulosic biomass utilization and lignin derivative materials, but very few studies are focused on the modification of lignosulfonate with ionic liquids or deep eutectic solvents. This finding led to an idea if deep eutectic solvents can dissolve or modify lignosulfonates: this became the central hypothesis of this thesis.

This thesis has two aims; first, it serves as a source of information on lignocellulosic biomass and on contemporary solvents, including ionic liquids and deep eutectic solvents. Secondly, this information is used in a study to learn about the properties of certain deep eutectic solvents and their ability to dissolve lignosulfonate.

Chapters 2 and 3 are focusing on the lignocellulosic biomasses and their properties in general: what is it composed of, what kind of chemical properties they have and so on. Chapter 4 is focusing on lignosulfonates and its properties. A broad overview of pretreatment methods of lignocellulosic biomass is presented in chapter 5, focusing on deep eutectic solvents in particular. In the experimental part (chapter 6) the dissolving properties of deep eutectic solvents are studied with a detailed study on their physiochemical properties. The experimental part is summarized in chapter 7: what were the findings of this thesis and how should the study be continued from this.

2 LIGNOCELLULOSIC BIOMASS

Lignocellulosic biomass, i.e., LCB, refers to any plant-based dry matter, it is the most abundant bio-renewable source of biomass on earth. The abundance of LCB makes it an excellent source of, for example, value-added fine chemicals and biofuels. Since LCB is a plant-based material, it is a carbon-neutral energy source. Wood is the primary source of biomass used today, Kindermann et al. (2008, 393) estimated that the annual world forest biomass growing stock is about 680 billion tons.

Biomass is still mostly utilized as a heating or energy source; it has long been recognized as a potentially sustainable source of sugars for biofuels and other bio-based materials. The increasing demand for consumer products and a lack of resources forces for a new way of thinking about how to produce a high-value product for consumers. Over the past years, extensive research has been done on LCB conversion into high-value products. One of the essential uses for biomass is the production of bioethanol, world annual production in 2016 reached a milestone of over 100 billion liters (Renewable Fuels Association 2018).

LCB is usually divided into three or four types by biological origin: softwood, hardwood, and grasses, sometimes the agricultural residue is counted as a fourth type.

2.1 Softwood biomass

The term softwood refers to specific wood from gymnosperm trees such as conifers. They do not have leaves, but needles and uncovered seeds that are produced in cones. The name softwood does not necessarily mean it is softer than hardwood. In both groups, the variation of actual wood hardness is enormous. For example, Douglas fir or yew are much harder than several hardwoods, and balsa, a type of hardwood, is softer than most softwoods. The number of known softwood species is around 1 000, which is relatively low compared to hardwoods (Stenius 2000, 13).

Softwoods, such as fir, pine, and spruce are the most common lignocellulosic feedstock in the Northern hemisphere; Table 1 summarizes a typical composition of these wood species. These are also the most important commercial trees for timber and wood-pulping production.

Table 1. Typical composition of common softwoods.

Softwood (Gymnosperm)	Cellulose %	Hemicellulose %	Lignin %
Douglas fir [1]	44	11	27
Pine [1]	42–50	24–27	20
Spruce [1]	46	23	28
Typical values [2]	**40-45**	**25-30**	**25-30**

[1] (Isikgor, Becer 2015, 4500), [2] (Stenius 2000, 28)

Woody biomass always contains extractives and inorganic substances, but the amount is usually only up to 5% in woods from the temperate zone, although tropical species can exceed this.

2.2 Hardwood biomass

Hardwood refers to an angiosperm, dicot trees. They produce covered seeds, have flowers, and broad leaves. The number of hardwood species is much more than softwood; it is estimated to be in the range of 30 000 - 35 000 (Stenius 2000, 13). The structure is more complicated compared to softwood, and the growth is slower as a result. The presence of pores, or vessels is the dominant feature separating hardwoods from softwoods. Table 2 summarizes the typical composition of these wood species.

Table 2. Typical composition of common hardwoods.

Hardwood (Angiosperm)	Cellulose %	Hemicellulose %	Lignin %
Poplar [1]	51-53	26-29	16
Oak [1]	40	36	24
Eucalyptus [1]	54	18	22
Typical values [2]	**40-45**	**30-35**	**20-25**

[1] (Isikgor, Becer 2015, 4500), [2] (Stenius 2000, 28)

Hardwoods contain in general more hemicelluloses compared to softwood but on another hand the fewer amount of lignin.

2.3 Grass and energy crop biomass

As indicated by the name, this group includes various types of grasses and energy crops, Switchgrass, Miscanthus, and Sorghum, to name a few. There are estimated to be over 11 000 known species of grasses worldwide (Mohapatra, Mishra et al. 2017, 1008, see, Clayton, Vorontsova et al. 2016). Typical commercial energy crops are densely planted, high-yielding crop species that are processed to bio-fuel and to produce energy.

Miscanthus (Miscanthus x giganteus) is probably the most commonly cultivated grass for cellulosic ethanol production. It can produce 5-8 times the amount of bioethanol per area as corn (Mohapatra, Mishra et al. 2017, 1009). Table 3 summarizes the typical composition of these species.

Table 3 Composition of common grasses and energy crops.

Biomass source	Cellulose %	Hemicellulose %	Lignin %
Miscanthus [1]	40	22	23
Sorghum Straw [2]	35	24	25
Switchgrass [3]	35–40	25–30	15–20
Typical values [4]	**35-40**	**22-30**	**15-25**

[1] (Han, Kim et al. 2011, 1944), [2] (Herrera, Téllez-Luis et al. 2003, 268), [3] (Isikgor, Becer 2015, 4500), [4] combined from [1-3] sources

There is an increasing research trend on the conversion of grasses into bio-fuel and other bio-based materials. Many kinds of grass can be cultivated in arid lands with minimal or virtually zero maintenance costs, though their annual production per area is not as attractive as the leading grass varieties, still, they possess a cheap source for biomass.

2.4 Agricultural residue

This group contains leftovers from agricultural production, for example, barley, rice, or wheat straws, sugarcane bagasse, or corn stovers. Corn, wheat, rice, and sugarcane are the four most cultivated crops. A typical composition of common agricultural residue is seen in Table 4.

Table 4. Average composition of different agricultural residues.

Biomass source	Cellulose %	Hemicellulose %	Lignin %
Sugarcane bagasse [1]	25-45	28-32	15-25
Corn stover [1]	34-41	17-36	6-18
Wheat straw [1]	35-39	23-30	12-16
Rice straw [1]	29-35	23-26	17-19
Typical values [2]	**25-41**	**17-36**	**6-25**

[1] (Isikgor, Becer 2015, 4500), [2] combined from source [1]

The composition of agricultural residues varies hugely, so a representative average value is not possible to give. In addition to compositional changes caused by different plant species, seasonal changes also affect the values significantly.

3 COMPOSITION OF LIGNOCELLULOSIC BIOMASS

Three main components of LCB is cellulose, hemicellulose, and an aromatic polymer called lignin, also smaller amounts of other compounds can be found, such as pectin, nitrogenous compounds, and ash (Chen 2014, 26, Stenius 2000, 12). Biomass is inherently recalcitrant towards processing, properties such as lignin content, cellulose accessibility to cellulase, and cellulose crystallinity determine the overall digestibility of the biomass (Agbor, Cicek et al. 2011, 677). The complex and heterogeneous structure of the plant cells' walls makes the development of efficient LCB utilization processes challenging.

3.1 Cellulose

The most substantial portion of the LCB is cellulose; the amount varies significantly depending on the source of the biomass. Typically, wood contains between 40-50% of cellulose by weight, whereas cotton can contain as high as 95%. Cellulose is a homopolysaccharide, with its backbone built from a linearly 1,4-ß-bonded glucopyranose unit, or glucose, forming a glucan polymer. The generalized molecular formula is $(C_6H_{10}O_5)_n$, where n stands for the degree of polymerization (DP), indicating the number of repeating polymer units (Anwar, Gulfraz et al. 2014, 164). The DP usually varies between 10 000-15 000 depending on its source. Figure 1 shows how every other glucose unit is rotated 180 degrees in the plane; the repeating disaccharide unit in cellulose is called cellobiose. Every glucose unit is connected to a single oxygen atom; this is called an acetal linkage.

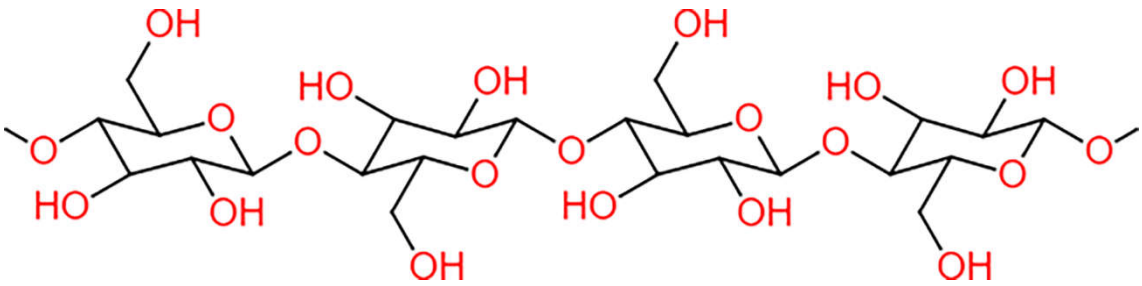

Figure 1. Chemical structure of cellulose. Redrawn according to (Chen 2014, 30).

Several glucan chains form a flat, inflexible, crystalline microfibril, held together by hydrogen bonds and Van der Waals forces. Cellulose fiber is composed of microfibrils entangled together, which makes the fibers stronger than steel wire of equal thickness. Unlike starch, cellulose is a straight polymer, with no coiling or branching. Cellulose fiber has a highly ordered crystalline region in the middle and a less ordered amorphous part in the end. The transition region from the crystalline to the amorphous part is not definite. Cellulose is strongly associated with hemicellulose and lignin (see chapter 3.3.2), due to this robust aggregation and a high degree of crystallinity, cellulose is nearly insoluble in most solvents (Ciolacu, Popa 2010, 3).

3.2 Hemicelluloses

Hemicelluloses are mixtures of amorphous polysaccharides, they have a lower molecular weight compared to cellulose (DP of 100-200), are more branched, and therefore have a higher solubility in solvents. Hemicelluloses are a combination of several different polysaccharides, mainly from hexose C6 sugars, glucose, galactose, mannose, and pentose C5 sugars, arabinose, and xylose. Some less common functional groups may also be present, such as acetyl and methyl groups, cinnamic, glucuronic and galacturonic acids. (Brandt, Gräsvik et al. 2013, 552.)

Hemicelluloses are relatively stable at high pH but are degraded more quickly in an acidic medium because of the low DP and few crystalline structures (Chen 2014, 45, Calvo-Flores, Dobado et al. 2015, 38). This is an essential feature to keep in mind while choosing the LCB deconstruction strategies.

Hemicelluloses can be classified into four different types, based on the polysaccharide composition of the backbone.

- Mannoglycans or mannans, present in secondary cell walls of softwood and Leguminosae
- Xyloglycans or xylans, present in secondary cell walls of hardwood and herbaceous plants
- Xyloglucans present in primary cell walls of higher plants and bound to cellulose
- Mixed-linkage β-glucans that are common in Poales and Pteridophytes

Table 5. Summary of most common hemicelluloses.

Source	Type	Main chain	Sidechain
Softwood	Galacto-glucomannan	Glucose and Mannose (1:3)	Galactose and acetyl group
Softwood	Arabino-glucuronoxylan	Xylose	Arabinose and uronic acid
Hardwood	Glucuronoxylan	Xylose	Galacturonic acid and acetyl group
Hardwood	Glucomannan	Glucose and Mannose (1:1-2)	Very little
Grass and Agricultural residue	Starch	Glucose	Glucose
Grass and Agricultural residue	Arabinoxylan	Xylose	Arabinose and little ferulic acid
Grass and Agricultural residue	ß-glucan	Glucose	Occasionally glucose

Table 5 summarizes the most common hemicelluloses found in LCB. These are described in more detail in the following chapters.

3.2.1 Softwood hemicellulose

Softwood hemicellulose is built mostly of galactoglucomannan (GGM), 15-20% of the dry wood mass. The backbone is built from ß-D-glucopyranose and ß-D-mannopyranose units, which are connected by 1,4-glycosidic bonds shown in Figure 2. Galactose is connected to the backbone as an α-D-galactopyranose group by a 1,6-glycosidic bond. Mannose is partially substituted at the C_2 or C_3 position with an acetyl group (Ac group in Figure 2). GGM has two fractions, the galactose-rich (two-thirds of the whole amount), and galactose poor fraction (one-third of the whole amount). Galactose rich fraction contains galactose, glucose, and mannose in the ratio of 1:1:3, and galactose poor fraction in a ratio of 0,1:1:3 (Stenius 2000, 36).

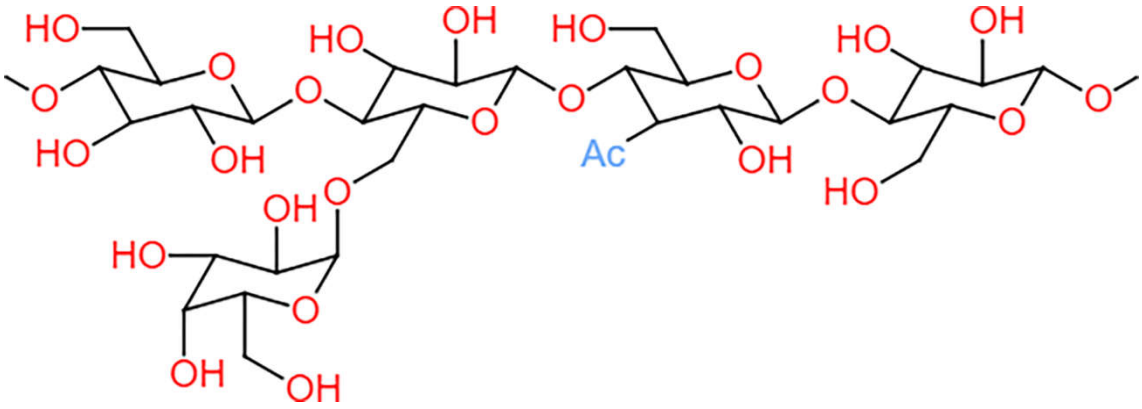

Figure 2. A typical structure of galactoglucomannan. Redrawn according to (Brandt, Gräsvik et al. 2013, 554).

Both GGM hemicelluloses contain acetyl side chains roughly 6% of the total GGM content, on average, one acetyl group per 3-4 hexose units (Stenius 2000, 37). GGM is easily depolymerized by acids, especially galactose side units are susceptible to hydrolysis. Acetyl groups are easily cleaved by even moderate alkalinity.

The second most abundant hemicellulose in softwood is arabinoglucuronoxylan (AGX), 5-10% of the dry wood mass, Figure 3 shows the structure of AGX.

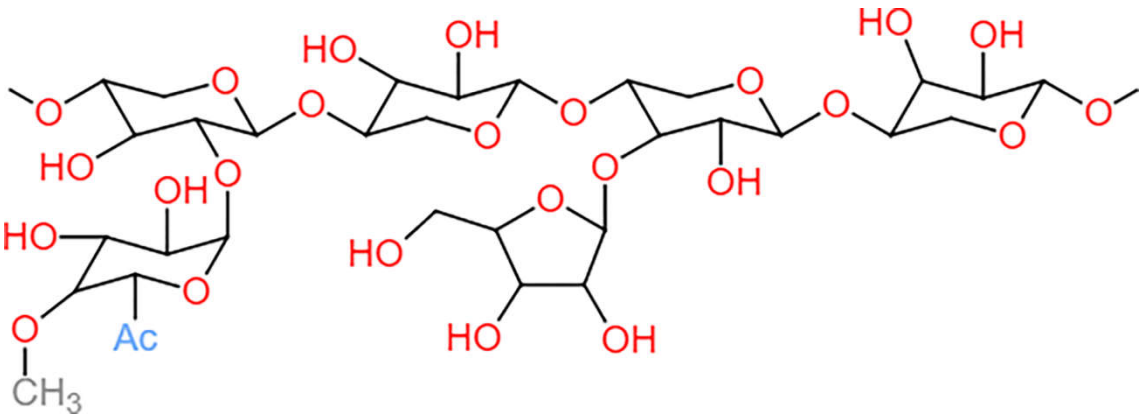

Figure 3. Structure of softwood arabinoglucuronoxylan. Redrawn according to (Stenius 2000, 36).

The backbone is ß-D-xylopyranose units, which are connected by 1,4-glycosidic bonds. The backbone contains 4-O-methyl-α-D-glucuronic acid moieties, or uronic acid, which are connected by 1,2-glycosidic bonds. Also, an α-L-arabino-furanose group is connected to the backbone by 1,3-glycosidic bonds. The ratio between constituents, arabinose, glucuronic acid, and xylose is 1:2:8, respectively (Stenius 2000, 37).

3.2.2 Hardwood hemicellulose

In hardwood, the primary hemicellulose is the glucuronoxylan (GX), in total 20-30% of the dry wood mass. It has the same framework as the softwood AGX (see Figure 3) but has less uronic acid substituents distributed unevenly along the xylan chain. The backbone moieties are partly acetylated at C_2 or C_3 position, on the average 3,5-7 acetyl groups per 10 xylose units (Stenius 2000, 37). Also, smaller amounts of L-rhamnose and galacturonic acids are present. The acetyl groups are hydrolyzed very easily by alkalinity; this is causing the high amount of acetic acid in birch sulfate pulping (Sjöström 1989, 65). The glycosidic bonds between xylose units are also easily hydrolyzed in acidic conditions, but the bonds between uronic acids and xylose are much more stable.

Secondary hemicellulose is the glucomannan (GM), less than 5% of the dry wood mass. It is similar to softwood GGM (see Figure 2), except it is not acetylated, is unsubstituted, and the glucose to mannose ratio is higher (1:1-2) (Sjöström 1989, 66). Acids more easily hydrolyze bonds between mannose units than glucose units, which promotes a positive effect towards depolymerization, compared to cellulose.

Some other miscellaneous polysaccharides, not all classified as hemicelluloses, are present in hardwood, for example, starch, callose, laricinan, xyloglucan, fucoxyloglucan, rhamnoarabinogalactan, and pectin.

3.2.3 Grass and agricultural residue hemicellulose

Starch is the main carbohydrate found in cereal grains; the amount can as high as 55-80% of the dry weight (Kulp 2000, 726). It contains two different polymers, linear amylose linked by α-1,4-bonds, and branched amylopectin linked by α-1,6-bonds, both polymers have a repeating glucose monomer as a backbone. Starch is usually utilized as a bio-ethanol production through acid or enzymatic hydrolyzation.

Arabinoxylan (AX) is the main hemicellulose naturally found in grasses, many cereals, and several agricultural residues, i.e., corn. ß-1,4-connected D-xylopyranose builds the backbone, with α-L-arabinofuranose side chains. These moieties can be substitutes in C_2 (Figure 4 blue) carbon, C_3 (orange) carbon or C_2 and C_3 (green) carbons. On occasion, these side-chains can contain esterified ferulic acid groups.

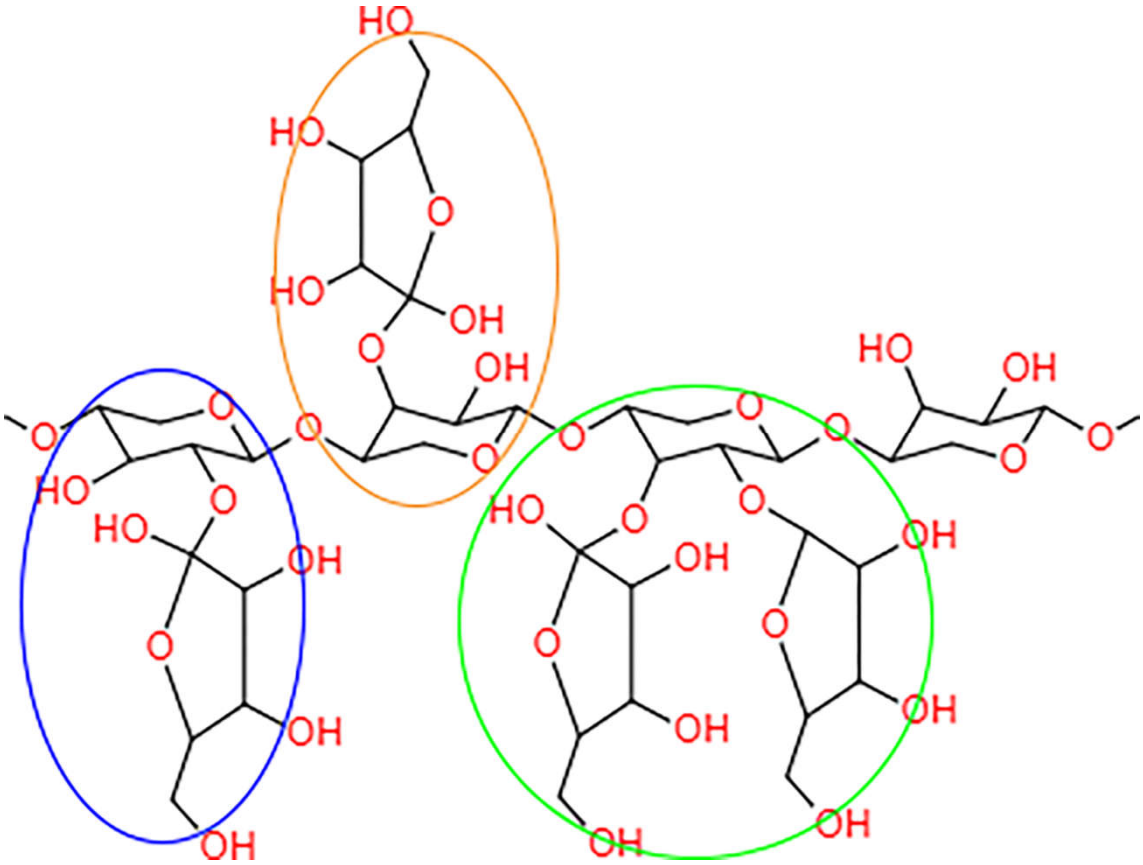

Figure 4. An example structure of arabinoxylan.

ß-glucan is a broad term covering many polysaccharides that are composed of β-D-glucopyranose units as the main building block. It has a similar backbone structure to cellulose, but it does not form crystal structures. ß-glucan can have a variety of different structures, but mostly it is built from ß-1,3 or ß-1,4-connected glucose units.

3.3 Lignin

Lignin is the second most abundant biopolymer found in nature after cellulose. The name lignin comes from a Latin word lignum, meaning wood. It is formed in the plant cells by the oxidative polymerization of three monolignols p-coumaryl, coniferyl and sinapyl alcohols; the process is called lignification (Isikgor, Becer 2015, 4500). As the plant cells mature, the cell wall becomes more lignified; this induces biomass recalcitrance. Although much of the lignin biosynthesis is understood, the exact mechanism is still not entirely resolved; this is caused by the difficulty of its study (Calvo-Flores, Dobado et al. 2015, 75).

Lignin has a different function in plants (Calvo-Flores, Dobado et al. 2015, 76):

- Lignin functions as the cellular glue which provides compressive strength to the individual fibers and the whole plant tissue.
- It prevents the cell walls from swelling in water, thus making the cells waterproof.
- Lignin serves as a barrier against microorganisms; lignified plant tissue is so compact that microorganisms cannot penetrate it.

Different plants contain varying amounts of lignin, but also the amount of lignin varies in different parts of the plant. Most lignin is in the secondary wall of the wood cells, although the concentration within is only around ~20%, the cells' large volume increases its amount to about ~80% of total lignin. The highest concentration (~70%) is found between adjacent cell walls, aka middle lamella, and the cell corners. (Saake, Lehnen 2007, 1.)

3.3.1 Chemical structure

The structure of lignin is amorphous, highly branched, and three dimensional, and it does not have an ordered or regular macromolecular structure. It composes of phenylpropane precursors; these phenolic compounds are hydroxycinnamyl alcohols or monolignols that share phenylpropane units and differs only in the degree of methoxylation (-OCH_3 group). These precursors are known as p-coumaryl, coniferyl, and sinapyl alcohols, as indicated in Figure 5. When these precursors exist in the polymer, they are called p-hydroxyphenyl (H), guaiacyl (G), and syringyl (S) residues, respectively. Other, less-abundant precursors have also been reported, with varying phenylpropane units or other functional groups. Due to the structural complexity of lignin, there is no commonly agreed structural model. The approximate elemental mass ratio (C:H:O) for softwood lignin is 64:6:30 and for hardwood lignin 59:6:35 (Stenius 2000, 40). Nomenclature is carried out by counting the connecting carbon atom from the benzene ring (1-6) and similarly from the carbon chain (α-γ), i.e., β-O-4 linkage (see Figure 6A).

Figure 5. Three lignin precursors. Redrawn according to (Calvo-Flores, Dobado et al. 2015, 13).

The first step in lignin polymerization is the dimerization of two monolignols, p-coumaryl, coniferyl, and sinapyl alcohols can polymerize from the benzene ring from 4, 3 or 2 different position respectively. For example, when two coniferyl alcohol radicals react, they have 15 different combinations, of which only 5 are stable (Calvo-Flores, Dobado et al. 2015, 89). When these dimers react again to form new radicals, the number of possible combinations is vast; this is the basis for the complexity of the resulting lignin. Monolignol dimers are then polymerized further by oxidative coupling to form a complex and branched structure, the exact method is still not wholly understood, and many different theories exist (Calvo-Flores, Dobado et al. 2015, 75). Lignin has been known since the 1840s and studied continuously then. A fitting example of the difficulty of this task is the finding of the so-called dibenzodioxocin structure by a Finnish group in 1995, which is today proposed as the main branching point in softwood lignin.

3.3.2 Lignin-carbohydrate complex

Björkman was the first to suggest the term Lignin-carbohydrate complex or LCC in his studies in 1954. Lignin is closely associated with carbohydrates, particularly with hemicelluloses, within vascular plant cell walls. Unlike hemicellulose's hydrogen bonds to cellulose, lignin is covalently bonded to carbohydrates, from α-carbon and C-4 in the phenylpropane benzene ring; this association is called the LCC. Numerous studies have been done to identify the exact linkage; most common linkage types are phenyl glycoside bonds, benzyl esters, benzyl ethers, and hemiacetal or acetal bonds. Many of the LCC linkages are easily cleaved off in alkalic or acidic conditions. (Stenius 2000, 42, Ghaffar, Fan 2013, 272, Calvo-Flores, Dobado et al. 2015, 38.) Brandt, Gräsvik et al. (2013, 552) suggested that the affinity of hemicellulose to lignin is enhanced by the substitution with hydrophobic groups, such as acetyl and methyl groups, and thus aids the cohesion between the three major lignocellulosic polymers.

3.3.3 Molecule weight

Stating the exact molecular weight of lignin is impossible because of the origin of lignin, depending on the plant species, the isolation method, and numerous different analytical techniques. The commonly used parameter is the weight average molecular weight (M_w or WAMW). However, it is common to use the number-average molecular weight (M_n or NAMW) in addition to M_w. Different studies suggest that the M_w of lignin, in general, is in the range of 10^3-10^5 daltons (Da), for softwood higher than $2x10^4$ Da, and hardwood less than that. Lignosulfonates can be as high as 10^6 Da (Calvo-Flores, Dobado et al. 2015, 40).

3.3.4 Dispersity index

The commonly used parameter is the dispersity index; it is a measure of the width of molecular weight distribution. IUPAC has replaced the term polydispersity index with a term dispersity index, represented by the symbol Đ (pronounced D-stroke), which is expressed in Equation 1. Dispersity index is always over 1, as the M_w cannot be lower than M_n. A high dispersity value means a broad distribution, usually indicating that severe degradation of lignin has taken place.

$$Đ_M = \frac{M_w}{M_n}$$

Equation 1. Dispersity index. (Calvo-Flores, Dobado et al. 2015, 40.)

An extensive amount of experimental data supports the idea that lignin shows remarkable dispersity, see Table 6. and Table 7. Numerous studies have been done on M_w, M_n, and $Đ_M$ of softwood and hardwood lignin. Table 6. recaps the effect of three conventional isolation methods, milled wood lignin (MWL), cellulolytic enzyme lignin (CEL), and enzymatic mild acidolysis lignin (EMAL) on M_w, M_n, and $Đ_M$ parameters. The isolation method has a significant impact on these parameters.

Table 6. Effect of isolation method on different softwood lignin.

Lignin source	Isolation method	M_n, g·mol^{-1}	M_w, g·mol^{-1}	$Đ_M$
Norway spruce	MWL[1]	6 400	23 500	3,7
	CEL[1]	9 450	53 850	5,7
	EMAL[2]	10 000	83 200	8,3
Douglas fir	MWL[3]	2 500	7 400	3,0
	CEL[3]	5 500	21 800	4,0
	EMAL[2]	7 700	49 500	6,4
Southern pine	MWL[3]	4 700	14 900	3,2
	CEL[3]	7 500	29 600	3,9
	EMAL[2]	9 760	57 600	5,9

[1] (Guerra, Filpponen, Lucia, Saquing et al. 2006, 5943), [2] (Guerra, Gaspar et al. 2007, 2575), [3] (Guerra, Filpponen, Lucia, and Argyropoulos 2006, 9700)

A generalization can be made from these results indicating that M_w decreases in the following order EMAL>CEL>MWL. For example, the M_w of Douglas fir was 49 500, 21 800, and 7 400 in respectively, and $Đ_M$ was 6.4, 4.0, and 3.0 in respectively. The changes between EMAL and MWL are significant. Still, MWL is generally considered as a representative model of native lignin's chemical structure and reactivity, even when the milling breaks up covalent bonds in the structure and lowers the M_w, M_n, and $Đ_M$ (Tolbert, Akinosho et al. 2014).

Table 7. M_n, M_w, and $Đ_M$ of two different lignin. (Glasser, Barnett et al. 1983, 927.)

Lignin source	Isolation method	M_n, g·mol^{-1}	M_w, g·mol^{-1}	$Đ_M$
Pine	Organosolv	500	1 400	2,8
	Kraft	1 300	4 300	3,3
	MWL	1 300	11 400	8,8
	Acid hydrolysis	800	40 000	50
Aspen	Organosolv	600	2 100	3,5
	Steam explosion	800	2 300	2,9
	Acid hydrolysis	660	10 100	15,3

Glasser et al. compared different isolation methods for Pine and Aspen's lignin reviewed in Table 7, M_w for MWL Pine lignin (11 400) is in the same range as for Southern Pine (14 900) as shown in Table 6, indicating a comparable figure. Comparing the figures, a general order for these methods is seen: Acid hydrolysis>MWL>Kraft>Steam explosion/Organosolv. This could also be viewed as the order of destructive effect on lignin. Studying the values of M_w and $Đ_M$ from Table 6. and Table 7. reveals a clear correlation between these values when M_w increases, so do $Đ_M$, Glasser, Davé et al. (1993) found similar kind of results.

3.3.5 Solubility

Native lignin is mostly insoluble in conventional organic solvents. Björkman was one of the first in 1956 to study lignin solubility, he studied milled wood lignin and found out that more than 50% of lignin residue is soluble in aqueous dioxane, due to the partial degradation by the physical transformation. During the milling process, covalent bonds are broken, and lignin fragments are created, therefore giving a lower M_w. Thus, in order to solubilize lignin, a fragment with lower M_w is needed. Reviewing Table 6 and Table 7 in respect of M_w, a lignin solubility can be estimated to be increasing as the M_w decreases, this was confirmed by Sameni, Krigstin et al. (2017).

3.3.6 Chemical classification

The chemical properties and structure of lignin depend on the plant species from which it was separated. Classification of lignin can be done in two different ways, either based on plant taxonomy or a chemical approach. Plant taxonomy method classifies lignin in the following three categories:

- Gymnosperm (Softwood), contain mostly G-type lignin
- Angiosperm (Hardwood), contain mostly G-S type lignin
- Grass, contain mostly G-S-H type lignin

Due to the fact of many exceptions in this classification, a more robust classification has been done based on a chemical approach. Softwood lignin is mostly composed of guaiacyl, a hardwood from a mixture of guaiacyl and syringyl, and grass lignin from a mixture of all three types. The distribution of different components is given in Table 8.

- Type G
- Type G-S
- Type G-S-H
- Type G-H

Table 8. Distribution of lignin precursors from different lignin sources.

Lignin source	p-coumaryl alcohol (H) %	Coniferyl alcohol (G) %	Sinapyl alcohol (S) %	S/G ratio
Softwood[1]	<5	>95	0	0[3]
Hardwood[1]	0-8	25-50	45-75	0,9-3,0[3]
Grasses[1]	5-35	35-80	20-55	0,3-1,6[3]
Sugarcane bagasse[2]	2	38	60	1,6
Sugarcane straw[2]	4	68	28	0,4

[1] (Belgacem, Gandini 2008, 203), [2] (del Río, Lino et al. 2015, 332), [3] calculated from the values of Belgacem et al.

The agricultural residue contains a varying amount of each lignin precursor. Sugarcane is in this case used to indicate different types, the fibrous fraction following juice extraction (bagasse), and the harvest residue (straw).

Table 9. Distribution of linkage types in different lignin sources.

Linkage-type	Dimer structure	Soft-wood[1]	Hard-wood[1]	Grass[2]	Energy crop[3]
Ether or carbon-oxygen bonds					
β-O-4	Phenylpropane β-aryl ether	45-50	60	77	82-84
α-O-4	Phenylpropane α-aryl ether	6-8	7	2	-
4-O-5	Diaryl ether	4-8	7	-	-
Carbon-carbon bonds					
5-5	Biphenyl and dibenzodioxocin	18-25	5	3	-
β-5	Phenylcoumaran	9-12	6	11	10-11
β-1	1,2-Diaryl propane	7-10	7	3	-
β-β	β-β-linked structures	3	3	4	6-7

[1] (Sjöström 1989, 79), [2] (Sun, Sun et al. 2005, J. Zeng, Helms et al. 2013), [3] (Wang, Bauer et al. 2012)

Separated lignin differs chemically and physically from native lignin because the delignification process modifies the structure. Most known fractioning methods reduce the amount of β-O-4 linkage, reduction of the linkage increases the depolymerization byproducts and leads to a loss of native-type lignin (Brandt, Gräsvik et al. 2013, 554). Table 9 summarizes the distribution of each lignin linkage type in several different lignin sources.

Guaiacyl units tend to form carbon-carbon cross-linking at the C-5 position. Therefore, softwood lignin has a higher amount of C-C bonds, while syringyl units in hardwood lignin are substituted at the C-5 position (see Figure 5). The C-C linking is chemically very stable, and thus it cannot be readily hydrolyzed by acids or bases, making delignification of softwood more difficult than for hardwood or grasses (Brandt, Gräsvik et al. 2013, 553). A large amount of methoxyl units in softwood lignin makes it less condensed and chemically more convertible (Calvo-Flores, Dobado et al. 2015, 102).

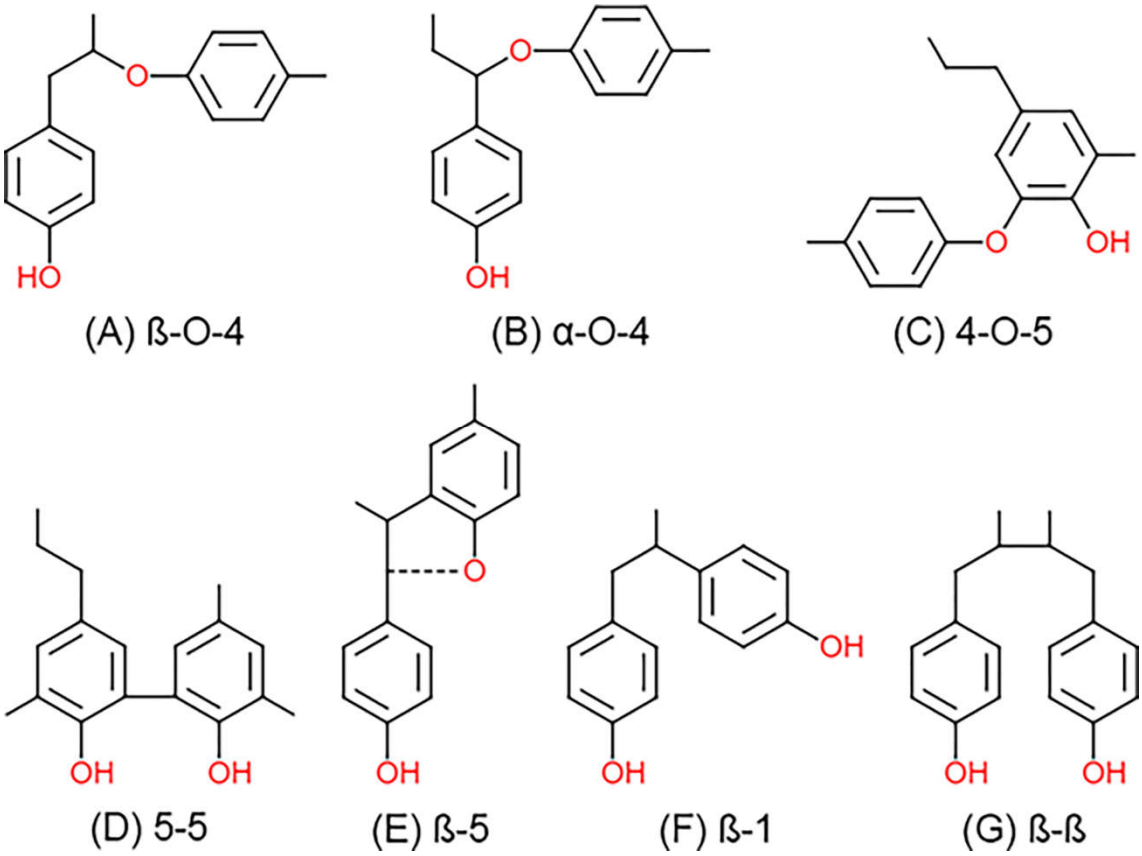

Figure 6. Common types of lignin linkage. Redrawn according to (Stenius 2000, 41)

The most common lignin linkage types and frequencies are shown in Table 9. Linkages are visualized in Figure 6, types A-C are ether bonds while D-G are carbon-carbon bonds.

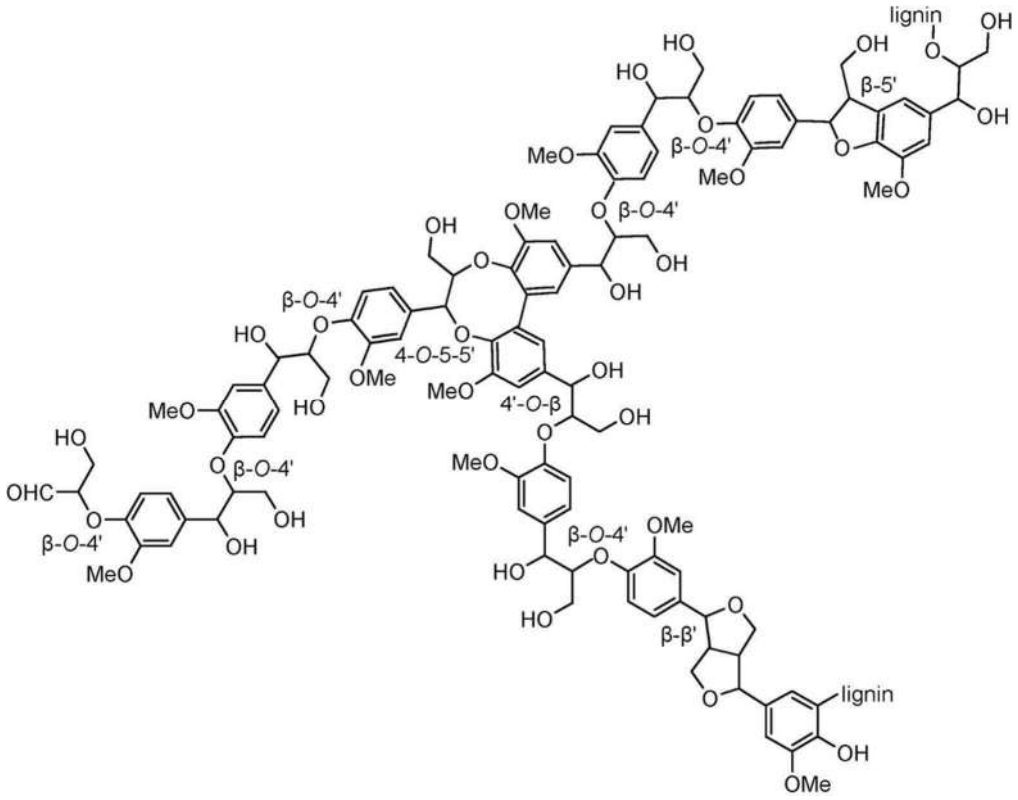

Figure 7. Contemporary View of Lignin Substructures. (*Contemporary View of Lignin Substructures.* 2006).

Figure 7 shows a fragment of softwood lignin; its complexity and diversity are visible as numerous different linkage types are presented in the structure (e.g., β-O-4, β-β, β-5). The 4-O-5-5' linkage in the middle presents the dibenzodioxocin structure, and it can be seen how the branching is happening from this point.

3.3.7 Model compounds of native lignin

Finding a representative model compound of native lignin has incited much research over the last decades. There is still today no accurate model found, due to its complex nature and inherent analytical difficulties. The first model for softwood was proposed already in 1968 by Freudenberg; it consisted of 18 monolignol units. Numerous different and more complex models have been suggested over the next decades by many

different researchers. Adler proposed in 1977 a model for spruce lignin based on oxidative degradation experiments. This model is partially limited, because some units and linkages cannot be accounted precisely, despite the limitation, this is structurally among the most extensive model, and one of the most widely used (Calvo-Flores, Dobado et al. 2015, 21-22). A significant part of the built models are softwood models with only a few hardwood models, or herbaceous models, the main reason for this is the inconsistency of hardwood lignin between species and the structural and chemical complexity of hardwood lignin. For herbaceous models, there is no commonly accepted structural model accurately describing this type of lignin. Also, no pure lignin model can represent the actual LCC aggregation with hemicelluloses.

An ideal model compound would be immensely complex, because several constraints would have to be met, such as:

- Right amount and distribution of linkages, e.g., β-O-4, β-5
- Condensed structure, affected by the number of methoxyl groups
- Carboxyl groups, present in 4-O-5 linkages
- Lignin-carbohydrate complexes
- Syringyl to guaiacyl ratio (S/G)
- Phenolic-OH groups

Each constraint is affected by numerous other parameters, such as the type and source of lignin, age of the plant, location of the lignin within the plant's cells. These constraints render the creation of a representative model compound of lignin virtually impossible.

4 LIGNOSULFONATES

Lignosulfonates are produced by the sulfite pulping process, which was patented in the United States already in 1866 by chemist Benjamin Tilghman using calcium bisulfite. The first commercial pulping plant was built in Sweden almost a decade later in 1874, and it used magnesium as the counter ion instead of calcium. The sulfite process quickly became the dominant pulping process until the 1940s when the sulfate or kraft process surpassed it. According to CEPI (2018, 8), in Europe, less than 5% of all produced pulp was of sulfite type. The main reasons for the kraft process's popularity are excellent pulp properties, lower environmental impact, and a broader variety of usable wood species.

The sulfite pulping method is based on the use of a bisulfite solution as a delignifying agent. The active sulfur-containing chemicals in the process are sulfur dioxide (SO_2), hydrogen sulfite ions (HSO_3^-), and sulfite ions (SO_3^{2-}). Common cations are calcium, sodium, magnesium, or ammonium. pH range and base ions can be seen in Table 10.

Table 10. Sulfite pulping processes. (Stenius 2000, 79.)

Process	pH range	Base	Active reagent
Acid sulfite	1-2	Na^+, Mg^{2+}, Ca^{2+}, H_4N^+	HSO_3^-, H^+
Bisulfite	2-6	Na^+, Mg^{2+}, Ca^{2+}, H_4N^+	HSO_3^-, H^+
Neutral sulfite (NSSC)[1]	6-9	Na^+, H_4N^+	HSO_3^-, SO_3^{2-}
AQ alkaline sulfite[2]	9-13	Na^+	SO_3^{2-}, HO^-

[1] Neutral sulfite semi-chemical, [2] Anthraquinone

Several different reactions take place during the acidic cooking phase; the primary reactions are sulfonation, hydrolysis, and condensation. Sulfonation leads to the generation of hydrophilic sulfonic acid groups by cleavage of α-hydroxyl or α-ether groups (see Figure 8). During hydrolysis α-aryl ether linkages are broken between the phenylpropane units of lignin, this causes the average molecular weight to decrease and creates new free phenolic hydroxyl groups. Both reactions increase the hydrophilicity of the lignin and promote its water solubility. The detrimental condensation reactions generate new stable carbon-carbon linkages between the phenylpropane units, therefore increase the M_w of the lignin, and decreases the water solubility (Stenius 2000, 83). The condensation reaction is blocked if the reactive groups of lignin are protected by sulfonation.

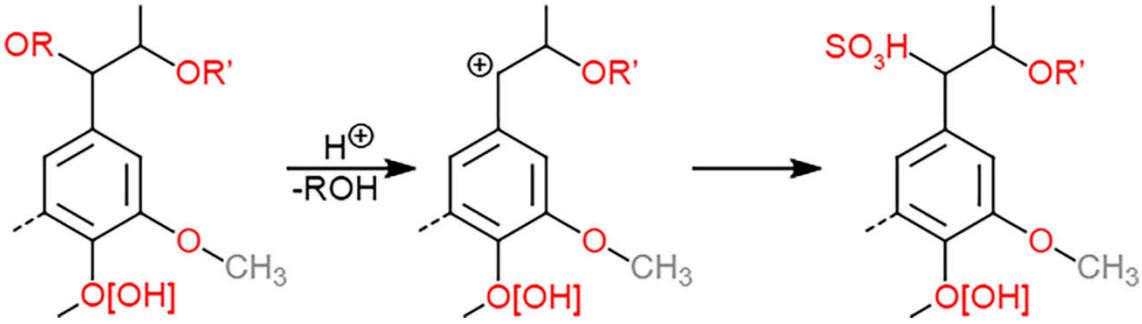

Figure 8. Sulfonation reaction of lignin in acid sulfite pulping.[1] Redrawn according to (Stenius 2000, 82).

[1] R indicates either a hydrogen or aryl group, R' indicates an aryl group

The cellulose remains unchanged through the reaction, while hemicelluloses are degraded into oligo- and monosaccharides. These sugars can then be separated from the spent liquor, but it is often tempting to burn the liquor due to its high energy content (Stenius 2000, 85). In principle, most wood types can be used with the sulfite pulping process. However, e.g., Pine and Douglas fir can cause problems because they contain pinosylvin and taxifolin, which can cause harmful cross-linking reactions with lignin, thus inhibiting the delignification, this issue is solved when two-stage cooking is used. Lignosulfonate sulfur content is 4-8 wt% of (Calvo-Flores, Dobado et al. 2015, 131).

Usually, the cooking is done in one stage, but two or three-stage cooking profiles with different pH regions are developed to enhance desirable pulp properties. Precooking can be done in the two-stage application, first in pH 6-7, and then use an acidic condition in the second stage. Sulfonation takes place in the first stage to a certain degree, while lignin is still retained in the wood phase. While in the second stage, the actual delignification is achieved. The two or three-stage pulping process dramatically improves the uniformity of lignin sulfonation. During the first stage, the reactive groups of lignin are protected by sulfonation, which causes condensation reactions to be blocked. (Stenius 2000, 79-80, Belgacem, Gandini 2008, 226-227.)

The rate of sulfonation in acid and bisulfite pulping is high, while in neutral or alkaline sulfite pulping it is low. The degree of sulfonation of lignin is expressed as the molar ratio of sulfonic acid groups to lignin methoxyl groups (SO_3H/OCH_3), which is for undissolved lignin or most NSSC lignin ~0.3, whereas for dissolved lignin it is about 0,5 or more. The degree of sulfonation for hardwood lignin is lower compared to softwood lignin, but it has the same type of difference. (Stenius 2000, 81, Belgacem, Gandini 2008, 226-227.)

5 PRETREATMENT METHODS

A pivotal bottleneck to biomass utilization is the inherent recalcitrance; this can be overcome by selecting a suitable pretreatment method. Research in the past decade has boomed in this field. When making a search in ScienceDirect with keywords “biomass” and “pretreatment” or “pre-treatment,” nearly 80 000 journal articles are found, with a substantial portion of them in the past decade. Some methods have apparent advantages over others, but so far, no method has prevailed as a suitable method for all biomasses. A chosen pretreatment method also dictates the available products and by-products that can be produced. Combining several pretreatment methods can enhance biomass digestibility, and wide-ranging conditions can be used while minimizing the formation of degradation products (Agbor, Cicek et al. 2011, 683). It should be pointed out, that achieving, for example, high sugar and ethanol yields is not the difficulty, but to obtain it with low energy input and thus with low capital and operational costs is. Efficacy of pretreatment step depends on many different parameters; standard parameters are (Agbor, Cicek et al. 2011, 677):

- Low capital and operational costs
- Wide range and loading of biomass
- Recovery of most LCB components in the usable form
- Minimized precondition step needs (size reduction)
- Very little or no degradation products
- Low energy demand or recirculation of energy to secondary purposes

Over the past century, starting from commercial pulp production, numerous different preprocessing methods have been studied and are still actively developed. Probably the most researched field are ionic liquids, deep eutectic liquids, and low melting mixtures (Ruß, König 2012, Procentese, Johnson et al. 2015, Yoo, Pu et al. 2017). The difficulty is the evaluation and comparison of different methods, due to upstream and downstream processing costs, capital investments, chemical recycling, and so on (Agbor, Cicek et al. 2011, 677). There are numerous ways to divide the pretreatments methods into groups, in this work, a division to chemical, physicochemical, physical, and biological is used as proposed by Kumar et al. (2017).

Table 11. Overview of biomass pretreatment methods. (Kumar, Sharma 2017, 3.)

Chemical	Physicochemical	Physical	Biological
Deep eutectic solvents	Ammonia-based	Mechanical extrusion	Archaeal
Dilute acid	CO_2 explosion	Microwave	Bacterial
Ionic liquids	Liquid hot water	Milling	Brown Fungi
Mild alkali	Oxidative pretreatment	Pulsed electric field	Fungi
Natural deep eutectic solvents	SPORL	Pyrolysis	Soft rot fungi
Organosolv	Steam explosion	Ultrasound	White fungi
Ozonolysis	Wet oxidation		

Due to the sheer number of available methods in Table 11, some cropping must be done for this work. Only three methods from the table are chosen for closer study in this thesis: ionic liquids, deep eutectic solvents, and natural deep eutectic solvents, also, based on research finding a low-temperature melting mixture is included in this work.

5.1 Ionic liquids

Ionic liquids are first mentioned in the literature in 1914, since the 50´s numerous research articles can be found, after the year 2000 the research has picked up an exponential growth. First ILs were considered as the new line of green solvents, but lately, many of them are proven not to be green at all (Paul, Moulik et al. 2015, xiii). They are called “designers solvents” because of a different combination of anions and cations that yields very different properties and characteristics, so they can be tailored to meet wanted specification.

ILs are formed by ionic bonding between bulky asymmetric organic cations, e.g., alkylated imidazolium, pyrrolidinium or pyridinium derivatives with weekly coordinating anions, like halides, alkyl sulfates, fluorinated hydrocarbons, carboxylic acids or amino acids. Typically, any salt that melts without decomposing or vaporizing can yield an ionic liquid. Generally ILs have been defined as liquid salt which has a melting point (T_m) of below 100°C (Wasserscheid, Welton 2008, 41); however, ionic liquids are now generally referred to as solvents which consist solely of ions (Smith, Abbott et al. 2014, 11062).

ILs have many interesting properties, including negligible vapor pressure, nonflammability, tunable physical properties, high ionic conductivity, and thermal stability. They also have several disadvantages compared to organic solvents, like high viscosity, difficult to synthesize, and toxicity. (Carlos Z. Andrade, Luana Alves 2005, 200.) Also, many IL applications require high solvent purity; their ionic structure can be adversely affected by the presence of any other ionic or molecular impurities including water (Francisco, van den Bruinhorst et al. 2013).

Predicting the melting point of a different combination of ILs is generally somewhat inaccurate, although Lazzús (2012) formed a generalized estimate for 200 ILs with an average deviation of only 7%. The size and symmetry of the anions and cations affect the melting point, the larger and more asymmetrical the ions are, generally the lower the melting point will be. For example, when a highly asymmetric cation 1-butyl-3-methylimidazolium is combined with asymmetric anion tetrafluoroborate, the resulting ionic liquid [BMIM]BF4 has a melting point of -71°C. De Gaetano et al. (2015, 66) found out that when the alkyl chain length of the cation increases, the melting and decomposition temperatures increased. When the chain length of alkylbetainium dicyanamide IL increased from 6 to 22 carbon atoms, the degradation temperature increased from 181 to 323°C.

5.2 Deep eutectic solvents

In early 2000 rose a new and exciting class of non-aqueous solvents, that cannot be identified as ILs, so-called deep eutectic solvents or DESs (Francisco, van den Bruinhorst et al. 2013, 3079). Unlike ILs, which forms binary ion pairs, DESs are formed by the complexation of a hydrogen bond-capable salt with a neutral hydrogen bond donor (Hammond, Bowron et al. 2016, 2736), and are thus mixtures, not ionic compounds. The first published paper presented on type III DES was in 2003 by Abbott et al. (2003). The general formula for a deep eutectic solvent is shown in Equation 2.

$$Cat^{+}X^{-}zY$$

Equation 2. The general formula for a deep eutectic solvent. (Smith, Abbott et al. 2014, 11061.)

Cat^{+} is an ammonium, phosphonium, or sulfonium cation, X^{-} corresponds to a Lewis base, usually a halide anion, and *Y* Brønsted acid, *z* referring to the number of *Y* molecules.

Deep eutectic solvents can be divided into four groups:

- Type I Quaternary ammonium salt + metal chloride
- Type II Quaternary ammonium salt + metal chloride hydrate
- Type III Quaternary ammonium salt + hydrogen bond donor
- Type IV Metal chloride hydrate + hydrogen bond donor

Type I DESs were first studied in the 60', due to the hygroscopic nature of halide metal salts, they were not air nor moisture stable (Wasserscheid, Welton 2008, 2-3), for this reason, the usability of these DESs are limited. However, these issues can be removed by using hydrated metal halide salts (type II), but they are not biodegradable nor environmentally friendly. Type IV DESs suffer from the same environmental and biodegradability issues than type II. Type III DESs are superior in many areas to all other types; they are not moisture or air-sensitive but are generally biodegradable and environmentally friendly. Type III is currently viewed as the most prominent and exciting type of DESs, mainly due to these facts and readily producible and low-toxicity starting materials. DESs have one significant advantage over ILs, simple mixing and heating of the starting material is enough, and the need for further purification is minimal.

5.2.1 Composition

Deep eutectic solvents can be produced from varieties of different components. Figure 9 presents a few common components, in the top, quaternary ammonium salts are shown, while the HBDs are on the bottom.

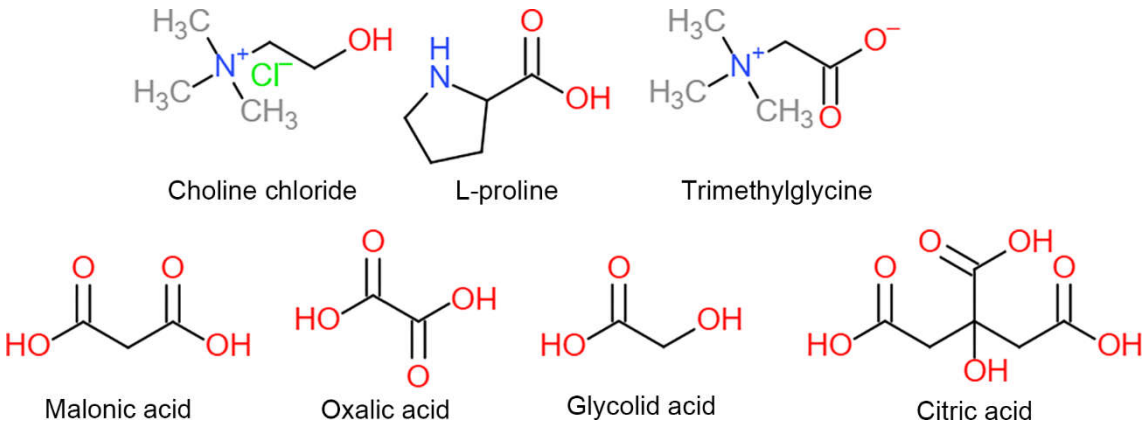

Figure 9. Standard DES components: quaternary ammonium salt (top row) and hydrogen bond donors (bottom row).

These few components present just a fraction of all the available components; it has been estimated that around 10^6 different theoretical combinations of DESs could be produced (Francisco, van den Bruinhorst et al. 2013). For this reason, DESs are called “designers solvents” because virtually any possible combination of properties could be achieved. This fact is far from the reality since only a handful of them are practical alternatives, and even fewer of those are studied. Their practicality is mostly controlled by the availability in large quantities for industrial-scale production.

Table 12. Reported eutectic composition of various DESs.

Salt	**HDB**	**Mole fraction of HBD, %**	**Mole ratio, Salt:HBD**
Betaine	Urea[1]	60	1:1,5
Betaine	Lactic acid[2]	50	1:1
Betaine	Oxalic acid·$2H_2O$[3]	67	1:2
Betaine	Citric acid·H_2O[3]	60	1:1,5

1 (C. Zeng, Qi et al. 2016), 2 (Yizhak 2018, 3), 3 (Cardellini, Tiecco et al. 2014, 55992)

Table 12 above shows a summary of the molar ratio of different DESs in eutectic composition. The component's chemical structure and its complexity, amount of hydroxyl and carboxyl groups, and hydration water influence the molar ratio liquid range. Francisco, van der Bruinhorst et al. noticed how the hydration water of oxalic acid betaine DES governs the liquid range, anhydrous oxalic acid did not form stable DES at a ratio of 1:1, but dehydrate oxalic acid did (Francisco, van den Bruinhorst et al. 2012, 2154).

5.2.2 The melting point and phase diagram

Shown in Figure 10, the melting point of the solution is decreasing as the mole fraction of B is increasing, to a point when it reaches a minimum, the eutectic point. In general, the higher the melting point of the pure salt, the higher the depreciation of melting point ΔT_m. This phenomenon arises from the lattice energy of the salt, salt with smaller lattice energy has a smaller interaction with the anion. (Smith, Abbott et al. 2014, 11063.)

Meng et al. (2016) studied the effect of water content to the melting point of ChCl:Urea DES, they noticed a decrease in melting point from 30°C down to 0°C, while the water content was increased from 0 wt% to 10 wt% respectively.

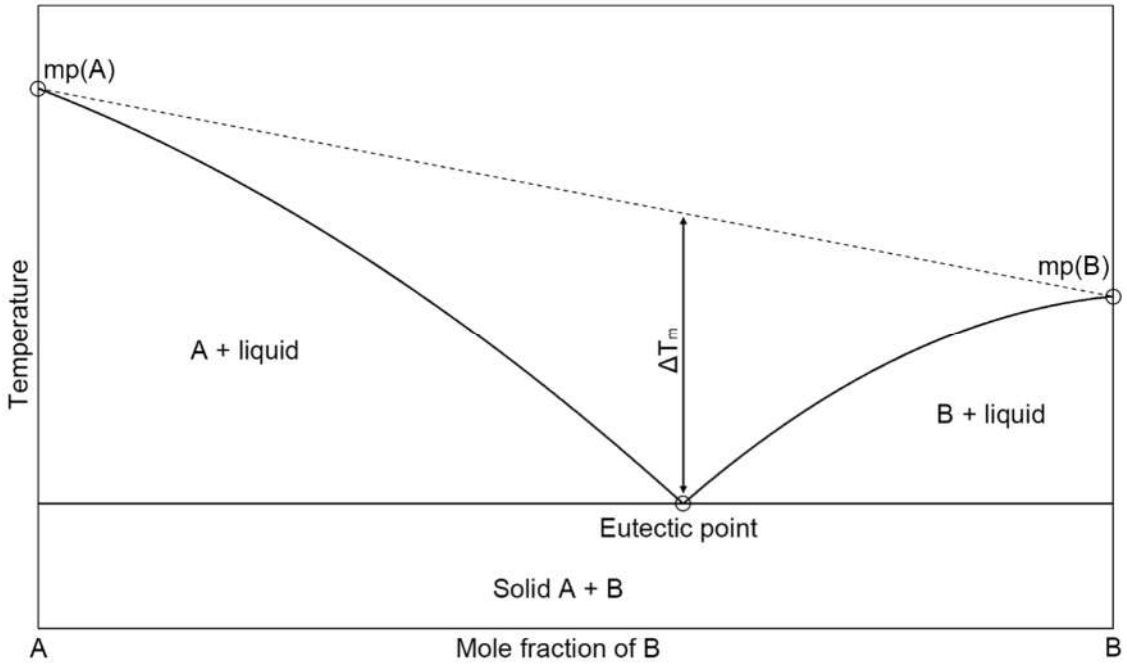

Figure 10. Example of the eutectic phase diagram of components A and B. Redrawn according to (Smith, Abbott et al. 2014, 11062.)

Unfortunately, in the literature melting point and freezing point are sometimes mixed. There can be a significant difference between freezing and melting point; the mixture can supercool before crystallization occurs (De Gaetano, Mohamadou et al. 2015, 65). A freezing point determination is ruled by, e.g., cooling rate, so melting point determination should be favored (Kick, Keil et al. 2013, 174). Although melting point and freezing point are inherently different, their change should be similar, i.e., when the freezing point of a DES is decreased by water addition, so should the melting point decrease.

Numerous studies have found out that DESs are very hygroscopic, Du, Zhao et al. found ChCl:Urea to absorb water up to 40 wt% from the open air at room temperature in 65 days. The DES could be quickly dried to 1,5 wt% by merely heating it at 60°C (Du, Zhao et al. 2016, 2). Studies show that the presence of water can lower the melting point of DESs (Meng, Ballerat-Busserolles et al. 2016, 4498). The temperature stability of DESs are found to be lower than of ILs, for example, ChCl:Urea DES is decomposing at 210°C, and DESs containing sugars usually decompose at 150°C (Ruß, König 2012, 2973).

5.3 Natural deep eutectic solvents

The term natural deep eutectic solvent or NADES was first coined by Choi et al. (2011, 1701) in 2011 to differentiate DESs of natural origin. Their team discovered more than 30 combinations of viscous liquids comprising of natural substances, between choline chloride, several carboxylic acids, and various sugars. So, in this respect, NADESs could be considered as a sub-category of DESs, although the definition of naturally occurring substances is vague. It seems fitting that the term NADES is used to distinguish solvents as genuinely green. Choi et al. (2011, 1701) interestingly found out that water can exist as part of the eutectic structure in choline chloride – water mixture with glucose, fructose, and sucrose. The water was not possible to be evaporated away as it was strongly retained in the mixture. Several studies have employed enzymatic reactions in DESs, Gorke et al. (2008) were the first to study this. The presence of urea or alcohols should disrupt the enzymatic activity or completely denature them, Gorke et al. hypothesize that a chemical potential of the components in DESs are lowered by a hydrogen-bond network formation and thus lower the disruptive behavior on enzyme reactions.

5.4 Low transition temperature mixtures

Low transition temperature mixtures (LTTM) or low melting mixtures (LMM) are liquids characterized by a decrease in melting point like DESs. According to Francisco et al. (2013, 3082), a distinguishing factor for LTTMs is the lack of melting point, which is replaced by a glass-transition temperature. This, however, can be somewhat confusing, in the literature, a mixture of ChCl and carboxylic acid are referred to as DES and LTTM depending on the author. Some mixtures exhibiting eutectic properties could be defined as LTTMs, such as sucrose:glucose:fructose, but this, however, was named as a NADES by Choi et al. (2011, 1702).

For clarification a classification between DESs, NADESs, and LTTMs could be as follows: DESs and LTTMs form two different groups, whereas NADESs would be a sub-group of DESs. A compound would be named DES if it follows the general equation of deep eutectic solvent Equation 2, NADESs are specifically type III DESs which are composed of natural origin substances, and LTTM could be all other compounds exhibiting eutectic behavior and not falling into DES or NADES categories.

5.5 Chemical properties

5.5.1 Viscosity

The viscosity of a substance or a mixture plays a vital role in practical applications; it has, e.g., a significant impact on the mass transport phenomena. The viscosity of ILs, DESs, and LMMs are of several magnitudes higher compared to water at the same temperature, reviewing the literature, it can range from 10 to over 10 000 mPas. Florindo et al. (2014, 2423) studied the differences in viscosities between DESs and ILs with the same ion counterparts; they found out the DES to have a lower viscosity in the range of 4-8 fold.

A so-called hole theory has been applied to ILs, DESs, and LTTMs to explain the viscosity and its temperature dependence. When an ionic material melts, hole theory assumes that it contains empty spaces caused by thermally generated fluctuations in local density. The holes are under constant flux and have random size and location. The size of the holes matches the size of the actual ions, so it is easy for a small ion to move into a vacant hole and therefore lower the viscosity of the liquid. When the temperature decreases, the holes grow smaller, and ions are less likely to move into the holes. Also, when the ions are bulkier and larger, it is increasingly difficult for them to move, this explains why the viscosities are higher for more complex ions. (Smith, Abbott et al. 2014, 11064.)

Generally, the viscosity of ILs, DESs, and LMMs is exponentially dependent on the temperature loosely following the Arrhenius equation (Equation 3).

$$\eta = \eta_0 \, exp\left(\frac{E_\eta}{RT}\right)$$

Equation 3. The Arrhenius equation. (Abbott, Boothby et al. 2004, 9144.)

The η denotes the viscosity, while η_0 is a constant, E_η is the activation energy, R is the universal gas constant and T the temperature in Kelvins. The Arrhenius equation assumes temperature-independent activation energy. While the Arrhenius equation usually produces adequate correlation, other, more accurate equations are a modification of it, for example, Litovitz (Equation 4) and VFT (Equation 5).

$$\eta = A\ exp\left(\frac{B}{RT^3}\right)$$

Equation 4. The Litovitz equation. (Ghatee, Zare et al. 2010, 3086.)

Litovitz equation is very similar to the Arrhenius equation, and it expresses a non-linear effect for the temperature. A and B are constants and T the temperature in Kelvins.

$$\eta = A\ exp\left(\frac{B}{T - T_0}\right)$$

Equation 5. The Vogel-Fulcher-Tammann equation. (Ghatee, Zare et al. 2010, 3086.)

Unlike the Arrhenius equation, the VFT equation proposes temperature-dependent activation energy. A and B are constants, T is the temperature and T_0 represents an ideal glass temperature. However, unlike in the Arrhenius equation, temperatures are expressed in °C, and thus the equation is only valid for $T>T_0$. In many publications, the VFT equation has produced the most accurate results.

The viscosity can be significantly reduced with water dilution; however, Hammond, Bowron et al. (2017, 9783) found out that the intense hydrogen interactions disappeared completely around 50 wt% dilution with water, a smaller amount ~5 wt% can be used without sacrificing the hydrogen bond network (Zhekenov, Toksanbayev et al. 2017, 47). The disappearance of hydrogen bondage at around 50 wt% could be seen as the transition phase from water-in-DES to DES-in-water.

5.5.2 Conductivity

Conductivity is probably the most frequently measured property of ILs, DESs, and LMMs, and it changes sharply with the composition and temperature of the mixture. Viscosity is strongly correlated with conductivity: the higher the viscosity, the lower the conductivity. The ion mobility and thus conductivity are determined by not only the availability of suitable holes but also the type and strength of ion−HBD interactions (Wasserscheid, Welton 2008, 110). Since the composition can affect the conductivity, it is practical to calculate a molar conductivity (Equation 6), which calculates the conductivity per mole of the solute (Wasserscheid, Welton 2008, 111).

$$\Lambda = \kappa \frac{M}{\rho}$$

Equation 6. Molar conductivity.

In equation Λ is the molar conductivity, κ denotes the conductivity, M a molar mass of the compound and ρ is the density. Numerous studies have utilized the Arrhenius, Litovitz, or VFT equations for modeling conductivity (Rengstl, Fischer et al. 2014, 22818).

5.5.3 Density

The density of ILs, DESs, and LTTMs generally change in the range of 1,0–1,3 $kg \cdot m^{-3}$ (Florindo, Oliveira et al. 2014, Lynam, Kumar et al. 2017, Zhekenov, Toksanbayev et al. 2017, Haghbakhsh, Raeissi 2018). Density does not usually exhibit as steep temperature dependency as the viscosity, but typically it is decreasing more linearly as the temperature increases. Numerous studies rely on linear correlation for the density, which can be calculated with Equation 7.

$$\rho = A + BT$$

Equation 7. A linear equation for density. (Florindo, Oliveira et al. 2014, 2421.)

In Equation 7, ρ denoted the density of the liquid, while A and B are constants, and T expresses the temperature in Kelvins. For more complex compound mixtures, the density does not always change linearly, so a second-order exponential equation can be used for better correlation as expressed in Equation 8.

$$\rho = exp(A + BT + CT^2)$$

Equation 8. Exponential second-order equation. (Haghbakhsh, Raeissi 2018, 12.)

In Equation 8, ρ denoted the density of the liquid, while A, B, and C are constants, and T expresses the temperature in Kelvins.

5.5.4 Ionicity

Numerous studies indicate a strong correlation for ILs between fluidity (reciprocal of viscosity) and molar conductivity (Λ), the same behavior has been observed with DESs and LMMs (Rengstl, Fischer et al. 2014, 22819). Due to the high viscosity, DESs and LMMs usually show a low conductivity. A Walden plot is a commonly used log-log plot of molar conductivity vs. fluidity, which indicates the degree of ionicity.

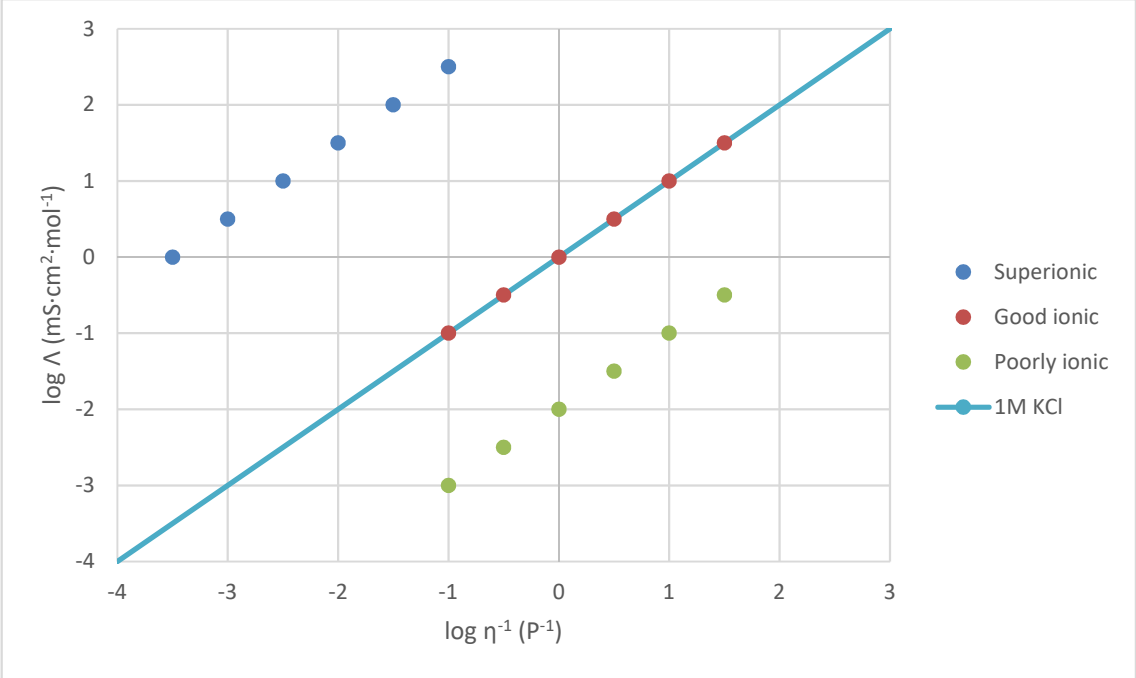

Figure 11. An arbitrary example of different ionic liquids.

Figure 11 shows how plots are compared against an 'ideal' case of 1M KCl, which exists as fully dissociated ions. A liquid closer to the KCl line is reviewed as an excellent ionic liquid. Liquids closer to the top left corner are considered superionic liquids because they have very high conductivity and viscosity. Liquids closer to the bottom right corner are poorly ionic or non-ionic liquids, and they have lower viscosity and conductivity. If needed, a simpler Walden plot can be drawn against conductivity rather than molar conductivity; however, this reduces the accuracy of the method.

5.5.5 Ultraviolet-visible spectroscopy

Ultraviolet-visible spectroscopy or UV-VIS for short is a method where the absorption or reflectance behavior of a substance is studied by ultraviolet and visible light. A light beam is directed through a sample, and the amount of light passed through is measured; thus, the sample absorbs part of the light. Generally, the ultraviolet light region falls in the range between 190-380 nm and the visible region fall between 380-750 nm. The Beer-Lambert law (Equation 9) states that the absorption is directly proportional to the concentration of the substance in the solution and the path length.

$$A = \varepsilon c l$$

Equation 9. Beer-Lambert law.

Each substance has its unique absorption properties, so to measure the amount of absorbing species in the solute, a molar attenuation coefficient must be known or calculated. In Equation 9, A stands for a measured absorbance, ε is the molar attenuation coefficient, c is a molar concentration, and l is the optical path length.

6 EXPERIMENTAL PART

The purpose of this part was to prepare several cheap and green deep eutectic solvent, measure their physical parameters, and study their ability to dissolve different sediments found from the Danisco Sweeteners Austria plant at Lenzing Austria. Six DESs containing betaine or trimethylglycine (TMG) as a quaternary ammonium salt was prepared. Tests were conducted for Danisco Sweeteners Oy (DWS) in Kantvik Finland between August 2018 and February 2019. Two sediment samples were acquired from the Lenzing plant. Table 13 present the prepared DESs in this work and their composition.

Table 13. Prepared DESs, their molar ratios, and target water percentages.

Compound	Sample name	Molar ratio	Water mass %
Betaine:Urea:Water	BE:UR	1:1,5:1	8,0
Betaine:Acetic acid	BE:AA	1:2	0,0
Betaine:Citric acid:Water	BE:CA	1:1,5:5	18,2
Betaine:Lactic acid	BE:LA	1:2	8,3
Betaine:Oxalic acid:Water	BE:OA	1:2:5	23,3
Betaine:Formic acid	BE:FA	1:2	0,0

Water content for samples BE:AA and BE:FA was assumed to be zero since the precursors were above 99% purity, and no suitable analysis method was available to verify the water content. The sample BE:LA contained water in the precursor; therefore, it contains a small amount of water.

6.1 Materials

Chemicals were partially purchased, Betaine (purity 99,7%) was donated from Finnfeeds Finland Oy in Naantali. The citric acid (Jungbunzlauer) and acetic acid (J.T.Baker, purity 99,7%, water content 0-1%) were acquired from the DSW laboratory. Oxalic acid (Acros Organics, purity 98%), lactic acid (Fisher Chemicals, purity 88%, water content 13,6%),

urea (Acros Organics, purity 99,5%), and formic acid (Acros Organics, purity 99%, water content 0-1%) were purchased from Fisher Scientific Finland.

Betaine, citric acid, oxalic acid, and urea were dried in a vacuum oven in 250 mbar pressure at 70°C temperature for at least 24 hours; otherwise, the chemicals were used without further purification.

6.2 Trimethylglycine

TMG, also called betaine or glycine betaine, is a quaternary ammonium salt like choline chloride. The term betaine refers to any neutral chemical compound with a positively charged cation functional group like quaternary ammonium or a phosphonium cation. Due to the established use in DSW, in this work, betaine refers solely to glycine betaine. Unlike choline chloride, betaine does not contain chloride as a cation, but it exists as a zwitterion, which is sometimes called an inner salt (see Figure 12).

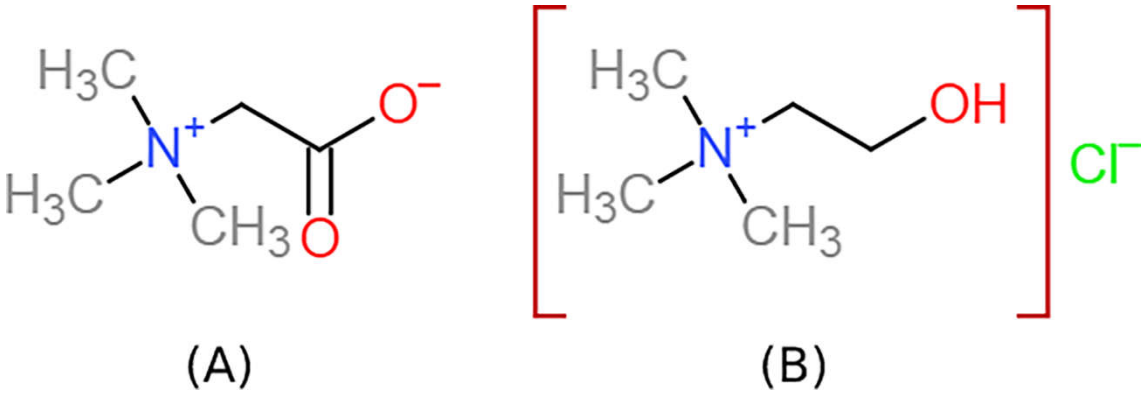

Figure 12. Chemical structure of Trimethylglycine (A) and Choline Chloride (B).

Betaine is the oxidation product of choline, where the two hydrogens are substituted by oxygen in the alfa carbon. Betaine has been successfully utilized in several studies as a part of ILs and DESs (Dai, van Spronsen et al. 2013, Cardellini, Tiecco et al. 2014, C. Zeng, Qi et al. 2016, Francisco, van den Bruinhorst et al. 2012).

6.3 Analysis of the prepared DESs

All analyses were done in the Danisco Sweeteners Oy laboratory in Kantvik. All other analysis, except HPLC and molar weight distribution, was carried out by the author.

6.3.1 Water content

The water content of the starting material and samples were analyzed with coulometric KF titration (Metrohm 851 titrando). Table 14 shows the measured water content, KF titration uses methanol as a solvent, which is incompatible with formic acid and acetic acid, so they were not measured and water content was assumed to be below 1%. After vacuum drying, all other starting materials were assumed to be dry.

Table 14. The water content of the starting material and samples.

Material	Water content, %	Standard deviation, %
Sample BE:UR	9,05	0,08
Sample BE:LA	7,91	0,01
Lactic acid	13,64	0,06

When the water content of BE:UR from Table 14 is compared to the target of 8,0 wt%, a comparable value is achieved, same applies to BE:LA when the water content is estimated from Lactic acid's water content, and molar ratio, a 7,2 wt% water content is achieved. These compare very well to the measured value, assuming some moisture absorption has happened during the sample handling, which is extremely hard to avoid without analyzing it under a nitrogen environment or in a glovebox.

6.3.2 Viscosity

The viscosity of the tested DESs was measured by Anton Paar RheolabQC rotational rheometer with a double-gap cylinder. The sample cylinder was temperature regulated by a jacketed heating vessel. Measurements were carried out in temperatures between 30-80°C. Different models (Equation 3, Equation 4, and Equation 5) were fitted to match the measured values by minimizing the root-mean-square error or RMSE. During sample preparation of BE:CA and BE:OA, a large amount of water needed to be added to get the samples dissolved. The viscosity was inspected visually and noted to be extremely high, so these two samples were discarded because the high viscosity made them unsuitable for further testing.

Results in Figure 13 shows how the structural complexity and amount of water in the mixture is affecting the viscosity. Formic acid assumes the most straightforward structural construction, followed by acetic acid and finally lactic acid. An apparent increase in viscosity can be seen with increasing structural complexity as assumed by the hole theory. Lactic acid is the only mixture of the three, which has water in the mixture, it can be estimated that waterless BE:LA mixture should have even higher viscosity. The structural complexity of urea lies somewhere between formic acid and acetic acid, which is reflected by a viscosity value in a similar range.

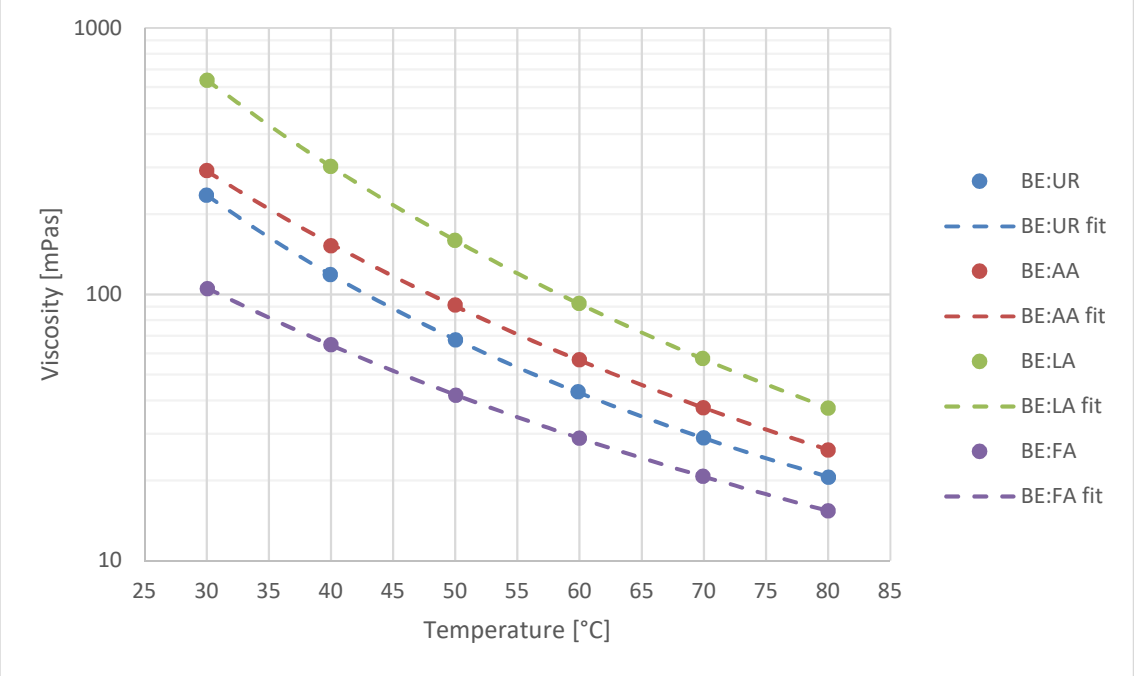

Figure 13. Measured and modeled (VFT) viscosities in different temperatures.

Table 15 shows the modeled viscosity values for BE:UR of Arrhenius, Litovitz, and VFT equations. Arrhenius equation seems to produce a rather large error, which is reduced by the Litovitz equation and even further by the VFT equation. Each of the four DES mixtures produced an error in a similar trend.

Table 15. Measured and modeled viscosities of BE:UR.

Temperature, °C	Measured, mPas	Arrhenius, mPas	Litovitz, mPas	VFT, mPas
30,0	235,6	210,4	223,4	235,4
40,0	118,8	122,2	121,3	118,8
50,0	67,4	73,1	70,5	67,7
60,0	43,0	45,5	44,1	42,8
70,0	28,9	28,8	28,8	28,9
80,0	20,6	18,8	19,7	20,6
RMSE	-	7,1	3,6	0,3

When using Arrhenius, Litovitz, and VFT equations for parameter fitting for all the samples, the lowest RMSE was achieved with VFT in all cases, and fitting parameters are presented in Table 16.

Table 16. Fitting parameters and RMSE of the VFT equation for viscosity.

Sample	η_0	E_η	T_0	RMSE, %
BE:UR	2,91E-1	586,69	-57,62	0,32
BE:AA	7,69E-2	996,34	-90,98	0,88
BE:LA	5,85E-2	1 060,44	-84,05	0,17
BE:FA	9,65E-2	921,59	-101,68	0,21

Overall, the viscosity measurement and modeling were very successful and accurate. VFT model proved to be most accurate, in all cases the RMSE was below one percent and usually around 0,2-0,3 percent.

6.3.3 Conductivity

The conductivity of the samples was measured with a Radiometer CDM92 conductivity meter with a model CDC641T measuring cell and the temperature with a Delta OHM HD 2307 handheld temperature probe. The sample temperature was controlled with a heatable magnetic stirring plate. The temperature was varied between 30-80°C.

When the results are fitted with previously introduced Arrhenius, Litovitz, and VFT equations, the best fit could be achieved with the VFT equation, results and fitting parameters are presented in Figure 14 and Table 17.

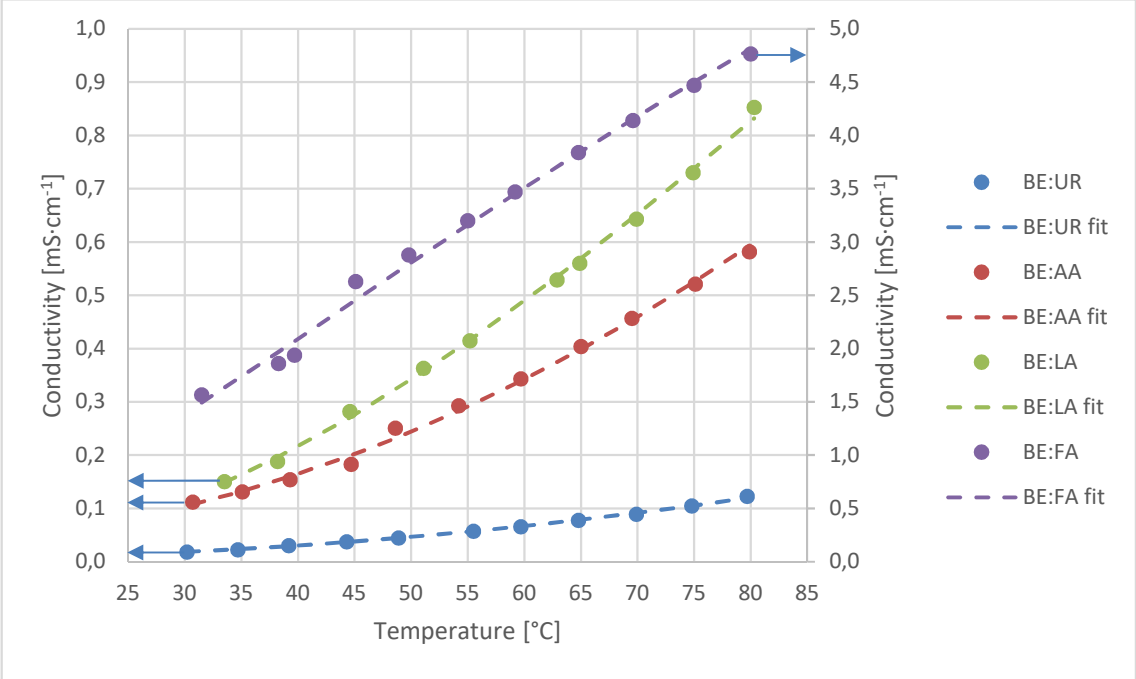

Figure 14. DESs conductivity at different temperatures.

All DESs with carboxylic acids as the HBD exhibit a temperature range between 38-49°C, where the conductivity increases sharply more than expected. This effect is most prominent in formic acid but is visible for acetic acid too, and only a minor increase can be seen for lactic acid. The cause for this effect can only be speculated, and it was not quantified in this study because it is out of the scope of this study.

Table 17. Fitting parameters and RMSE of the VFT equation for conductivity.

Sample	η_0	E_η	T_0	RMSE, %
BE:UR	6,49	-619,64	-75,41	1,98
BE:AA	31,11	-645,83	-83,21	4,20
BE:LA	9,23	-269,99	-31,88	2,20
BE:FA	17,74	-133,76	-22,55	3,79

Even when the VFT equation produces the results with the lowest RMSE, the error is about an order of magnitude higher compared those of viscosity, and it can be partly explained by the unexpected increase of conductivity in a specific temperature range, but also with the lower accuracy of the measurement instrument.

6.3.4 Walden plot

A Walden plot was calculated from the modeled viscosities and conductivities; Figure 15 shows the result. As discussed earlier, the Walden plot shows the ionicity of ILs, DESs, and LTTMs. Because no practical density measurement was available, the Walden plot is calculated against a measured conductivity, not against molar conductivity as usually done.

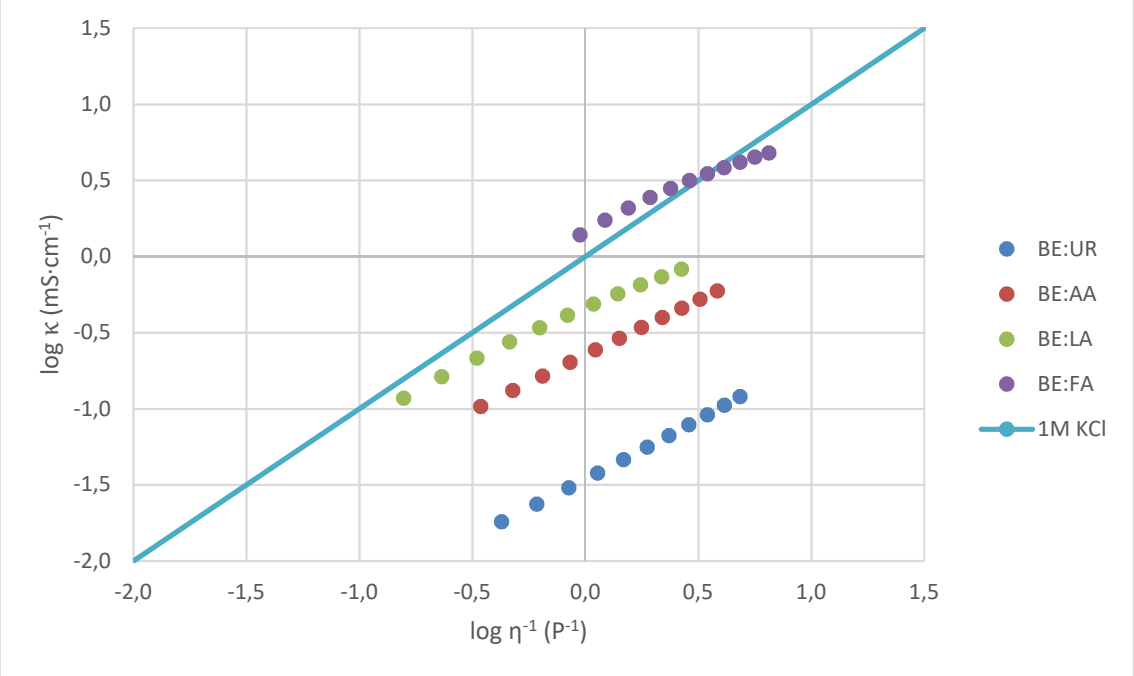

Figure 15. Walden plot of all four tested DES solutions.

The results show how all the carboxylic acid-based DESs are somewhat closer to each other, while BE:UR is far lower. This indicates BE:FA to be the most highly ionic of the measured samples, while BE:UR would likely to be weekly ionic. Based on the hole theory BE:LA line could be thought to be lower than BE:AA line, but due to the amount of water incorporated in it, the viscosity is lower, and conductivity is higher, and therefore its line is a bit higher than BE:AA

6.3.5 UV-VIS spectroscopy

All four prepared DESs were diluted into 10 wt%, and 1 wt% concentrations and their absorption were measured with Shimadzu UV-1800 spectrophotometer. Table 18 summarizes the data from the sample preparation for DES background testing.

Table 18. Summary table of the DES background testing.

	BE:UR		**BE:AA**		**BE:LA**		**BE:FA**	
Sample number	1	2	3	4	5	6	7	8
Dilution factor	101,03	10,13	100,04	9,98	101,06	10,02	103,14	10,29
Dry substance, %	91,6	91,6	100,0	100,0	92,4	92,4	100,0	100,0
Molar mass, g/mol	82,90	82,90	79,08	79,08	99,10	99,10	69,74	69,74
Concentration, mol/l	0,109	1,104	0,126	1,274	0,092	0,945	0,139	1,421

Each sample was scanned three times and averaged, abs values above 2.5, and below 0,025 were discarded to ensure reliable results. A scan was done from 190 nm to 400 nm, a 1cm thick cuvette was used with a built-in sipper unit. Figure 16 shows a molar absorption coefficient calculated as a function of wavelength for the undiluted sample.

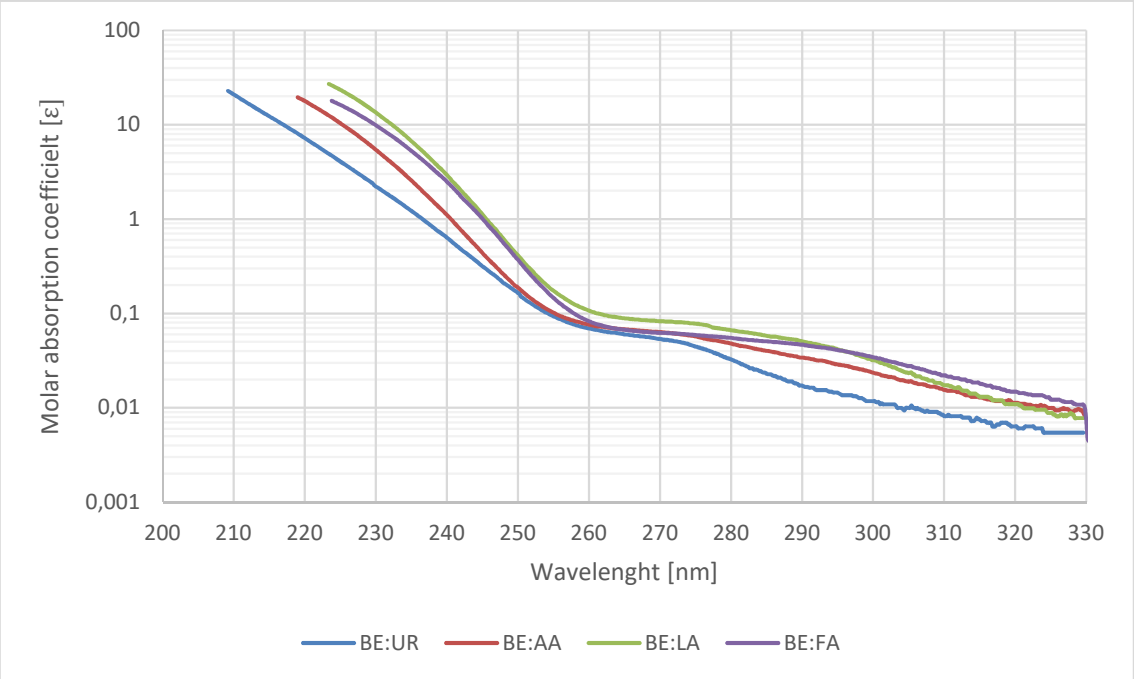

Figure 16. Background absorbance of tested DESs.

The molar absorption coefficient varies between the samples nearly 10-fold. All samples follow a similarly shaped curve where absorption decreases rapidly until about 260 nm. Wavelengths above 260 would be suitable for the concentration analysis of sediments in later chapters.

6.3.6 Distillation

BE:UR was chosen for distillation experiment since all of the tested carboxylic acids are volatile and they are not suitable for distillation but urea is non-volatile. A rotary vacuum evaporator (Büchi Rotavapor R-200) was used, a sample with a known water content was weighed in a glass evaporation flask. Evaporation was done at 70°C, the pressure was reduced once this temperature was reached. A vacuum was applied gently to prevent excessive boiling when no more boiling was observed at maximum vacuum a sample was taken for coulometric water content analysis, a maximum vacuum was 30 mbar absolute. Flask was weighed prior to sample taking and the evaporated water amount was calculated. Table 19 shows the dry substance content of feed and distillate achieved by vacuum distillation calculated by two different methods.

Table 19. The dry substance of BE:UR feed and distillate

Method	Feed	Distillate
Titration, ds%	83,1	94,0
Weighing, ds%	-	97,9

Distillation of BE:UR performed rather well and quite low water content was achieved, the sample stayed totally clear with no visible coloring taking place which shows that it's a stable compound under distillation. Weighing method probably gives more reliable results, since it was done immediately after distillation with minimal exposure, whereas titration method requires a lot of exposure to open air. Perhaps even lower water content could be achieved with higher temperatures and lower vacuum, but this experiment showed that BE:UR is easily distillable making it a versatile DES with easy dewatering method.

6.4 Sediment sample analysis

Two types of sediment were received from the Lenzing plant, one granular sample, and one scale type sample. These samples are named as furfural coal and lignosulfonate, respectively.

6.4.1 Furfural coal

The sediment is called at the Lenzing plant as furfural coal (Picture 1), in this study, furfural coal or abbreviation FC is used. The elemental composition was analyzed by Lenzing AG laboratory, and in this study, the breakdown can be seen in Table 20 and Table 21.

Picture 1. Dried furfural coal.

FC is found sedimented in pipes and bag filters. Usually, it is found in granular form, but over time, it can form a porous sponge-like solid hard matter (Picture 2).

Picture 2. Hardened furfural coal.

As the sample was thought to be organic, an excessive amount of carbon was expected. Surprisingly barium and sulfur were found in large quantities. Barium sulfate ($BaSO_4$) is usually found at the plant precipitated in pipes and tanks, it is near water-insoluble salt.

Table 20. Elemental composition of the furfural coal analyzed by Lenzing AG.

Element	Carbon (C)	Barium (Ba)	Magnesium (Mg)	Sulfur (S)	SUM
Weight %	95,2	1,8	0,5	2,1	99,6

Barium in the precipitate would most likely be present as barium sulfate, which would lower the sulfur amount by 0,4 wt% down to 1,7 wt%. When the FC was analyzed in more detail in this study (Table 21), no barium was found, although sulfur and magnesium amounts are similar than found in Table 20. Part of sulfur is in the sulfate (SO_4) group; this reduces the sulfur amount to 1,98 wt%.

Table 21. Elemental composition of the furfural coal.

Element or compound	Quantity, wt%	Element or compound	Quantity, wt%
Barium (Ba)	0,00	**Phosphate (PO_4)**	0,06
Calcium (Ca)	0,03	**Sulfur (S)**	2,34
Iron (Fe)	0,01	**Silicon (Si)**	0,01
Potassium (K)	0,06	**Sulfate (SO_4)**	1,07
Magnesium (Mg)	0,73	**Acetate**	0,61
Manganese (Mn)	0,01	**Citrate**	0,04
Sodium (Na)	0,16	**Formiate**	0,64
Phosphorus (P)	0,03	**Oxalate**	0,07
SUM	**5,88**		

The monosaccharide content of FC was analyzed with high-performance liquid chromatography (HPLC) technique; Table 22 summarizes the analysis results. The first sample was dissolved in ultrapure water under 30 minutes of sonication and filtered through a 0,2 µm syringe filter. The sample was heavily clouded, and much of the material was left insoluble in water. The second sample was dissolved in 0,1M NaOH, in which FC dissolved completely without any haze, the sample was neutralized by 1M HCl and filtered through a 0,2 µm syringe filter before analysis.

Results between water and NaOH soluble monosaccharide content are surprisingly similar, with only minor differences. The high amount of xylose is no surprise because the process liquid contains a high amount of monomer xylose. Also, other monosaccharides are found from the process liquid, and they are likely just trapped inside the dried granular particles and not a part of the sediment itself. The lack of furfural and HMF was not anticipated because the sample was expected to contain said components in particular. The compounds “Rt 10.6-12.6” and “Rt 15.1” refers to unidentified compounds of specific retention time.

Table 22. HPLC analysis of furfural coal.

Compound	Water-soluble, wt%	NaOH soluble, wt%
Rt 10.6-12.6	2,58	2,26
Glucose	1,26	1,19
Xylose	7,53	7,41
Rt 15.1	0,38	0,33
Galactose and Rhamnose	0,73	0,65
Arabinose	0,19	0,16
Mannose	0,88	0,87
Hydroxymethylfurfural (HMF)	0,00	0,00
Furfural	0,00	0,00
SUM	**13,55**	**12,87**

The combined amount of analyzed monosaccharides strongly suggests that a significant portion, about 87 wt%, of the sediment is of high molecular weight compounds, which cannot be analyzed by this HPLC technique. This why a size exclusion chromatography analysis was carried out to find out the molecular weight distribution. FC was diluted first in $LiNO_3$ which is used as an eluent in the analysis, sample dissolved partially, another sample was dissolved in 0,1M NaOH, where it dissolved completely. Figure 17 shows the chromatograms of $LiNO_3$ (top) and the NaOH (bottom) dissolved samples.

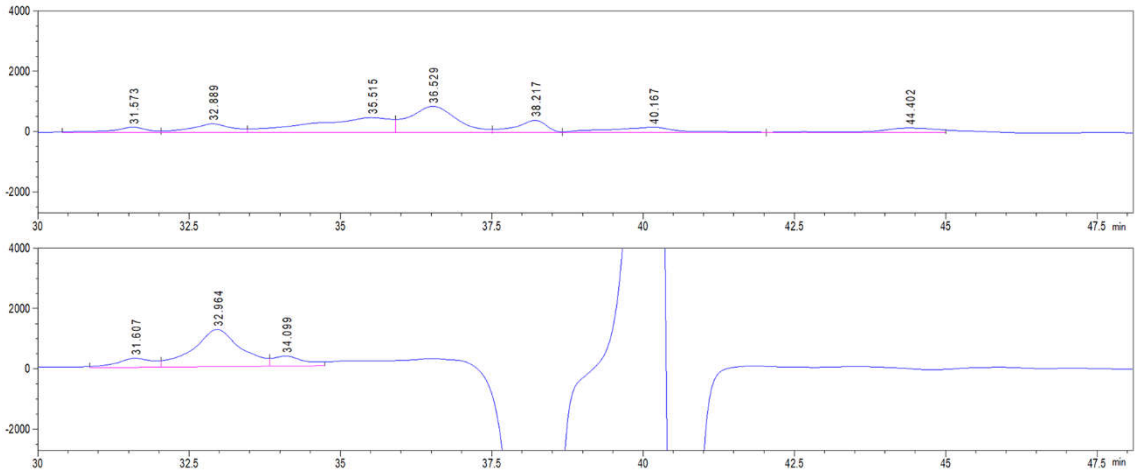

Figure 17. Molecular weight distribution chromatogram of furfural coal.

As mentioned above, the LiNO3 dissolved sample had lots of material undissolved, so very likely only the two most leftmost peaks with retention time 31,573 and 32,889 min are not identified by the HPLC analysis (Table 22). With the NaOH dissolved sample, a very high peak in 40 min region followed and preceded by a negative peak is caused by NaOH itself and this peak hides any other compounds which have a retention time between about 37-42 minutes. The three peaks before retention time 35 mins are the only compounds found from the NaOH dissolved sample.

Table 23 summarizes the retention times found from the M_w analysis. The retention time of reference samples was analyzed with M_w between 150-5900 $g \cdot mol^{-1}$; this allows us to estimate the M_w of the FC based on its retention time.

Table 23. Estimated M_w distribution of furfural coal.

Sample	**Retention time, min**	**Estimated M_w, $g \cdot mol^{-1}$**
$LiNO_3$	31,573	1 449
$LiNO_3$	32,889	705
	Average	**973**
NaOH	31,607	1 420
NaOH	32,964	678
NaOH	34,099	392
	Average	**746**

Both peaks in the $LiNO_3$ sample are very similar compared to the NaOH sample, so these peaks can be assumed to be the same. Under the right conditions, NaOH could break down the chemical structure of the sediment, but this does not seem plausible because the dissolution was very rapid, and no change in the sample was noticed. In addition, when the NaOH dissolved sample is neutralized below pH 11,0-11,5 a visible cloud point is reached, and part of the sample turns into a non-aqueous form.

6.4.2 Lignosulfonate

For this study, the scale type sample is named as lignosulfonate sediment, abbreviated as LS (Picture 3). This type of sample has been previously analyzed extensively by DWS. It was concluded that it composes most likely of lignosulfonate with a low degree of sulfonation and wood-based extractives co-precipitated with multivalent metals.

Picture 3. Lignosulfonate sample.

The degree of sulfonation, the ratio of sulfur and lignin, was 3,4 %, which indicates a lower level of sulfonation (see chapter 4), this decreases its water solubility. The molar mass distribution was M_n 2700, M_w 29800, and $Đ_M$ 11.0, this indicates a very broad distribution, typical for LS. The amount of lignosulfonate of the sample was 53,6 wt%.

6.5 The solubility of tested samples

6.5.1 Furfural coal sample

The solubility of FC was first tested with 0,1M NaOH and it was found out to dissolve completely in it. Sample dissolved into a very dark and clear liquid, no visual precipitation was observed. When this liquid was diluted with pure water, a brownish precipitate started to form. A series of different concentrations of NaOH solutions were prepared and FC was dissolved into them. Dissolver amount was 0,1 wt%. The results are seen in Table 24.

Table 24. Solubility scan of FC at different pH

Calculated solution pH	NaOH concentration, mol/l	Turbidity, NTU
11,0	0,001	94,8
12,0	0,01	28,9
13,0	0,1	7,3

A clear behavior was observed, the higher the pH the less turbidity was observed. Sample in pH 11,0 didn't dissolve completely. Due to an easy solubility, no further testing was done with DESs, this would not be a practical approach since mild NaOH was able to dissolve the sample completely.

6.5.2 Lignosulfonate sample

The LS sample was dissolved in 0,1M sodium hydroxide overnight at 80°C temperature; the amount was 500 ppm. Figure 18 shows the graph of absorbance and its derivative between wavelength 240 to 400 nm. Especially the absorbance curve shows very interesting local maximums and minimums, maximums are found at about 251, 295, and 345 nm, while 270 and 380 shows an explicit minimum. Jablonský, Kočiš et al. (2015) found for sulfonated kraft lignin remarkably similar peaks, maximums were noticed at 249, 304, and 351 nm, and a minimum at 279 nm. The small "bump" in the derivative curve at 340 nm is a result of the change of light source by the measuring instrument.

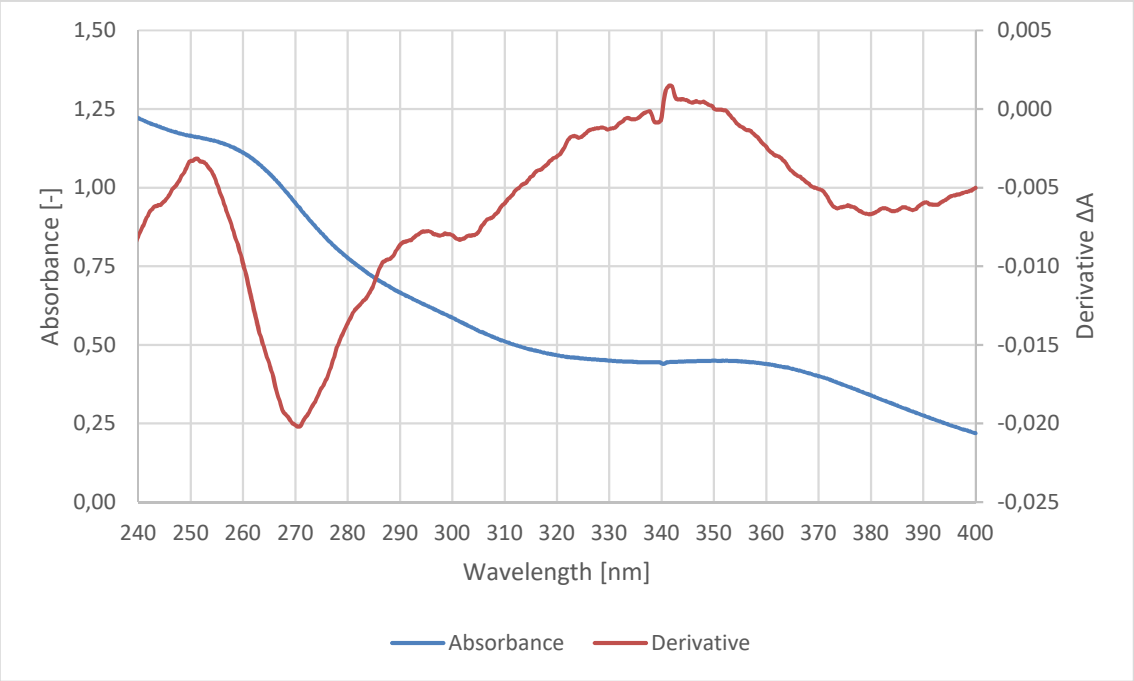

Figure 18. UV-VIS absorption curve of the lignosulfonate sample.

Around wavelength 340-350 nm is a very stable absorbance plateau, which can be used for absorbance measuring with a single wavelength, wavelength 345 nm was selected as a reference. Wavelength 295 nm would also allow the measurement to be carried out. Both wavelengths are far away from major interference DES absorbance wavelength, see Figure 16.

A molar attenuation coefficient for a reference material was calculated from the solution prepared earlier. Table 25 sums the measurement with different wavelengths and dilution factors. The sample was not completely clear, and it was filtered through a 0,45 µ syringe filter. It was assumed that all the LS was dissolved, and the haze was caused by other insoluble substances.

Table 25. A molar attenuation coefficient of the lignosulfonate sample.

Wave-length, nm	Dilution factor	Lignin amount, %	Optical length, cm	Absorbance	Sediment concentration, mol/l	Molar attenuation coefficient, $l \cdot mol^{-1} \cdot cm^{-1}$
251	9,9	53,6	1,0	1,161	9,02E-07	1,29E+06
251	5,0	53,6	1,0	2,343	1,80E-06	1,30E+06

An absorbance calibration curve is drawn from the values of Table 25. Figure 19 represents the absorbance as a function of concentration. When the curve is forced through the origin, the slope of the curve is the molar attenuation coefficient, which was 1 301 438 $l \cdot mol^{-1} \cdot cm^{-1}$.

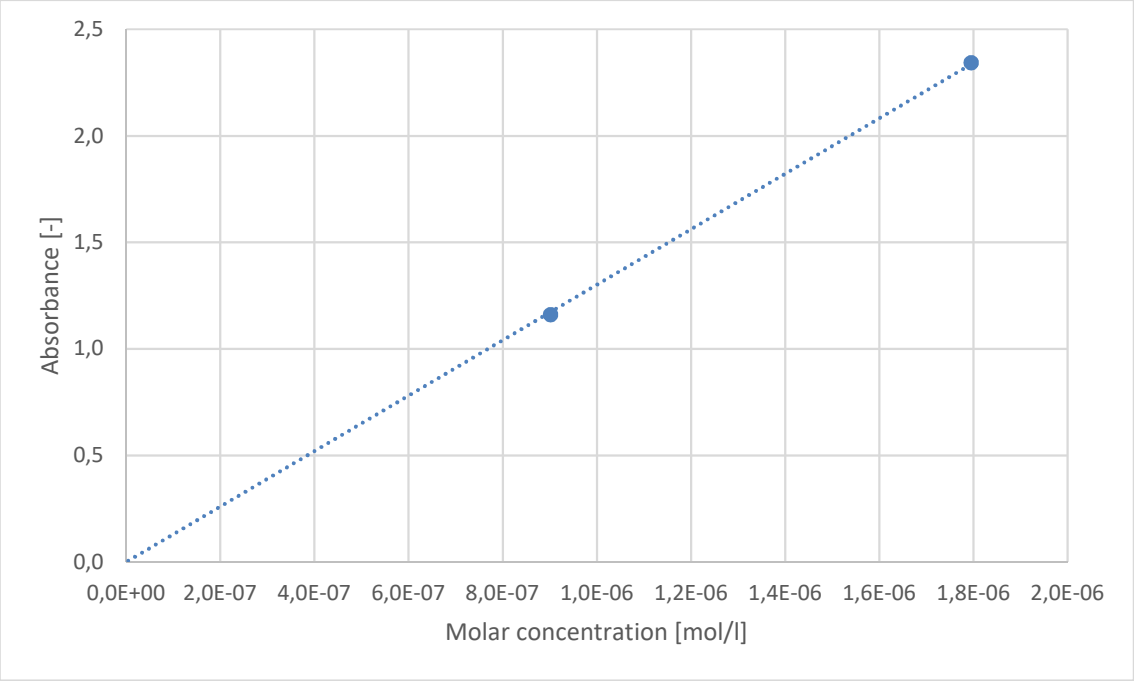

Figure 19. Absorbance calibration curve of the lignosulfonate sample.

The LS sediment was dissolved in the four tested DESs and their absorbance was measured. The concentration of 500 ppm or 0,5 g/l of sediment was weighed in a flask with appropriate DES, and the mixture was mixed in a water bath at 80°C for 24 hours. BE:UR was then diluted by a factor of 10 and 50, and the rest DESs by a factor of 10 and 30, the absorbance was measured from wavelength 190 to 400 nm.

The amount of dissolved LS was calculated at a wavelength of 251 nm with the calibration curve of the NaOH reference after background subtraction a corresponding DES molar absorption (see Figure 16). Table 26 shows the results. Pure LS amount was estimated assuming the precipitate contained 53,6% of lignosulfonate.

Table 26. Dissolved lignosulfonate.

Sample	BE:UR	BE:AA	BE:LA	BE:FA
Dissolved LS, mol/l	4,64E-06	2,26E-06	1,15E-06	7,62E-07
Dissolved LS, g/l	0,26	0,13	0,06	0,04
Dissolved pure LS, g/l	0,27	0,27	0,28	0,29
Dissolved pure LS, %	95,4	46,4	23,0	14,8

Surprisingly BE:UR sample was able to dissolve the sample virtually entirely, while the others only dissolve it partially. Due to measurement inaccuracy it can be questioned whether BE:UR truly dissolved only 95% of LS in the sample, or could it have dissolved even more. Figure 20 represents the calculated absorption curve of undiluted samples.

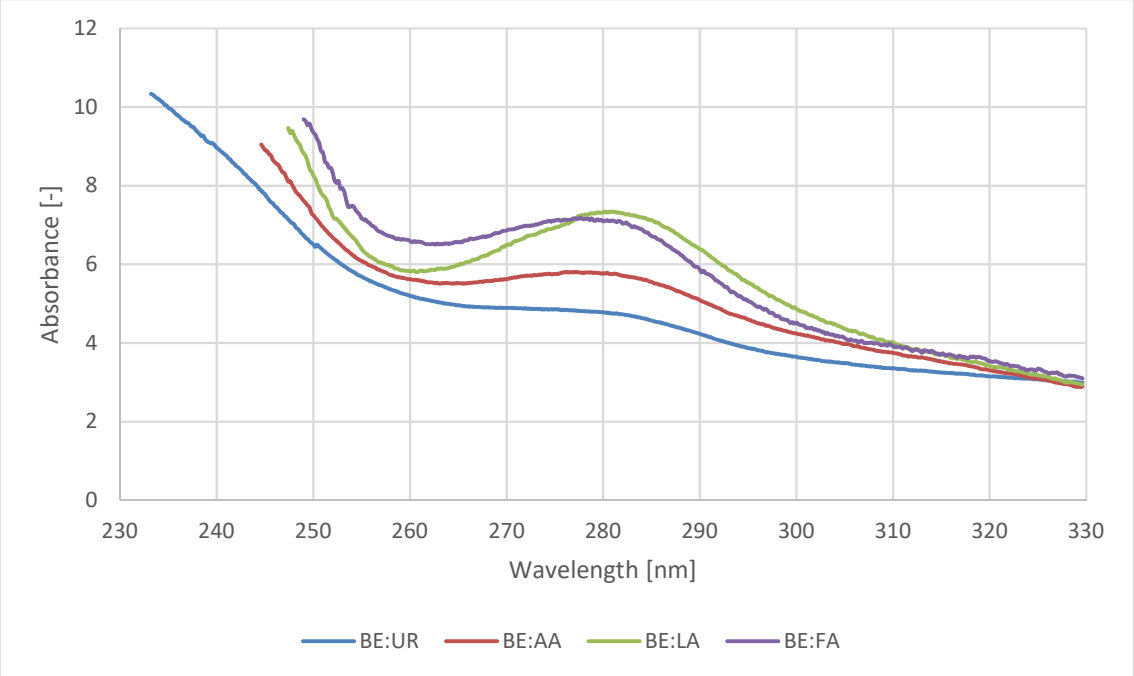

Figure 20. Absorption curve of dissolved LS in different DESs

The LS absorption curve is calculated for an undiluted sample and corrected for dissolved pure LS amount. All curves have a similar shape showing comparable values. Interestingly all curves show a local maximum at about 270 nm with different absorption levels. This clearly indicates a different kind of dissolving behavior between the DESs. Identifying the compound responsible for the absorption peak is out of the scope of this work, so more analysis of the absorption curve was not done.

During the dissolution test a visible coloring effect was also seen, displayed in Picture 4, from left to right BE:UR, BE:AA, BE:LA, and BE:FA correspondingly. The LS was dispersed entirely in all other samples other than BE:LA, the sample color seems to follow the amount of dissolved LS, smallest in BE:LA and BE:FA.

Picture 4. DES sample of the lignosulfonate dissolution test.

As discussed in chapter 5.5.4 a value closer to the 1M KCl reference line, i.e., a greater ΔW should indicate a stronger ionic compound. The stronger ionic compound could be assumed to have a better dissolving property. When a graph between dissolved LS and corresponding ΔW at the same temperature was done, a remarkably good fit was seen between these values, shown in Figure 21.

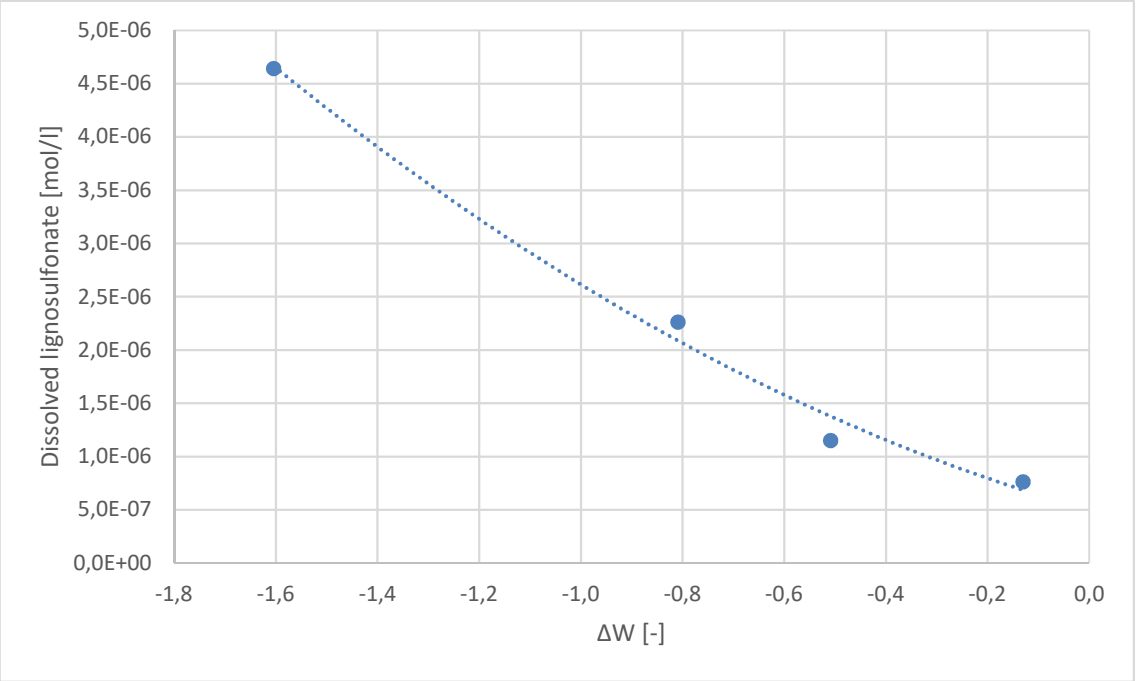

Figure 21. Correlation of ΔW and dissolved lignosulfonate.

Surprisingly Figure 21 indicates the opposite behavior. In this experiment, a smaller ΔW value is strongly correlated to a better dissolving property, Pearson correlation factor R^2=0,9904. Since BE:UR dissolved the sample virtually wholly, the exact amount is not known with confidence; thus in Figure 21, the leftmost data point could be higher. The exact reason for negative correlation remained unclear and no cause was found out. Identifying the cause for this remained outside of the scope of this work and it was not studied further.

7 CONCLUSION AND DISCUSSION

Six different DESs with betaine as a quaternary ammonium salt was produced in this study, two of them (BE:CA and BE:OA) were discarded from further testing due to extremely high viscosity. The physical properties of the remaining four DESs were studied and analyzed.

The second part of the study was to analyze two sediments and investigate their solubility in the four previously prepared DESs. The lignosulfonate sediments had been previously studied extensively, but the furfural coal sediment was a new type. At the time of this study, no other studies were found investigating DES between betaine and formic acid, or to study the solubility of lignosulfonate in any of the four DESs.

7.1 DES properties

Viscosity, conductivity, and water content of four prepared DESs were measured. A Walden plot was drawn, which indicated a difference in their ionicity, BE:FA being the most strongly ionic and BE:UR the most weakly. Although the plot does not take a molar conductivity into account, a direct conductivity instead, it still gives an excellent relative indication between the four tested DESs. The order of ionicity of the carboxylic acids is clearly explained by the size of the HBD and the number of available hydrogen atoms capable to form hydrogen bonds. The low ionicity of BE:UR can be explained by the weaker hydrogen bond of NH−O compared to BE:FA OH−O bond and a small HBD size. In general, viscosity is decreasing as the HBD gets smaller, as per the hole theory, but the strength of the hydrogen bond increases viscosity and conductivity. This why BE:UR has a high viscosity but a low conductivity, whereas BE:FA has a low viscosity and a high conductivity. Overall it was proven that betaine can form deep eutectic solvents with various HBDs.

A distillation experiment showed that BE:UR is easily distillable as low as 2,1 wt% water content. DES being distillable is a very interesting and usable ability, because distilling allows an easy dewatering method down to very low water content without losing or degrading the starting materials.

7.2 Sediment properties

A furfural coal sediment was analyzed, its chemical composition and molecular weight distribution were measured. The chemical composition indicates that only 13 wt% of the sample was identified, mainly being xylose. This suggested that the rest of the material has a higher molecular weight. The average molecular weight of 750 g/mol was measured, the NaOH analysis was chosen over the $LiNO_3$ because NaOH dissolved the whole sample. It seems clear that the water-insoluble part is the actual sediment and the rest is mainly part of the process liquor dried along with the sediment. The fact that the sediment was so easily soluble in mild NaOH discouraged further testing of its DES solubility study; it would have no practical value dissolving it by DESs.

7.3 DES dissolution properties

Dissolution properties of the four previously prepared DESs were studied with two sediments found from Danisco Sweeteners xylose plant in Lenzing. Furfural coal was dropped from further dissolution studies, because of its easy solubility in mild NaOH liquid. All four tested DESs were able to dissolve the lignosulfonate sediment with varying degrees. BE:UR was found to dissolve LS completely in the tested concentration of 500 ppm. Dissolution tendency decreased as a function of HBD in the following series; urea (UR)>acetic acid (AA)>lactic acid (LA)>formic acid (FA).

Very interesting behavior was noticed when a dissolution tendency was compared against DESs ΔW value; a clear correlation was found. The lower the ΔW value was, the better the DES dissolved the LS sample. This behavior was opposite to what it was hypothesized, making it a unique find in this thesis, the reason remained unclear.

7.4 A further point of interest

Since betaine was found out to easily form eutectic compositions with varying HBDs, this study can easily be continued to find out more betaine based DESs and to study their chemical properties. The correlation between dissolution ability and ΔW was a very interesting finding. This type of work can also be continued, but it would require quite an extensive background work to find out the actual reason for this behavior.

REFERENCES

Contemporary View of Lignin Substructures. 2006. U.S. DOE.

ABBOTT, A.P., BOOTHBY, D., CAPPER, G., DAVIES, D.L. and RASHEED, R.K., 2004. Deep Eutectic Solvents Formed between Choline Chloride and Carboxylic Acids: Versatile Alternatives to Ionic Liquids. *Journal of the American Chemical Society,* **126**(29), pp. 9142-9147.

ABBOTT, A.P., CAPPER, G., DAVIES, D.L., RASHEED, R.K. and TAMBYRAJAH, V., 2003. Novel solvent properties of choline chloride/urea mixtures. *Chemical communications (Cambridge, England),* (1), pp. 70.

AGBOR, V.B., CICEK, N., SPARLING, R., BERLIN, A. and LEVIN, D.B., 2011. Biomass pretreatment: Fundamentals toward application. *Biotechnology Advances,* **29**(6), pp. 675-685.

ANWAR, Z., GULFRAZ, M. and IRSHAD, M., 2014. Agro-industrial lignocellulosic biomass a key to unlock the future bio-energy: A brief review. *Journal of Radiation Research and Applied Sciences,* **7**(2), pp. 163-173.

BELGACEM, M.N. and GANDINI, A., 2008. *Monomers, Polymers and Composites from Renewable Resources.* Oxford, UNITED KINGDOM: Elsevier Science & Technology.

BRANDT, A., GRÄSVIK, J., HALLETT, J.P. and WELTON, T., 2013. Deconstruction of lignocellulosic biomass with ionic liquids. *Green Chemistry,* **15**(3), pp. 55-583.

CALVO-FLORES, F.G., DOBADO, J.A., ISAC-GARCÍA, J. and MARTÍN-MARTÍNEZ, F.J., 2015. *Lignin and Lignans as Renewable Raw Materials.* 1 edn. New York: John Wiley & Sons Inc.

CARDELLINI, F., TIECCO, M., GERMANI, R., CARDINALI, G., CORTE, L., ROSCINI, L. and SPRETI, N., 2014. Novel zwitterionic deep eutectic solvents from trimethylglycine and carboxylic acids: characterization of their properties and their toxicity. *RSC Adv,* **4**(99), pp. 55990-56002.

CARLOS Z. ANDRADE and LUANA ALVES, 2005. Environmentally Benign Solvents in Organic Synthesis: Current Topics. *Current Organic Chemistry,* **9**(2), pp. 195-218.

CEPI, 2018. *Key Statistics 2017.* Confederation of European Paper Industries.

CHEN, H., 2014. Chemical Composition and Structure of Natural Lignocellulose. *Biotechnology of Lignocellulose.* Springer, Dordrecht, pp. 25-71.

CHOI, Y.H., VAN SPRONSEN, J., DAI, Y., VERBERNE, M., HOLLMANN, F., ARENDS, ISABEL W. C. E., WITKAMP, G. and VERPOORTE, R., 2011. Are Natural Deep Eutectic Solvents the Missing Link in Understanding Cellular Metabolism and Physiology? *Plant Physiology,* **156**(4), pp. 1701-1705.

CIOLACU, D. and POPA, V.I., 2010. *Cellulose Allomorphs: Structure, Accessibility and Reactivity.* Hauppauge: Nova.

CLAYTON, W.D., VORONTSOVA, M.S., HARMAN, K.T. and WILLIAMSON, H., 2016-last update, GrassBase - The Online World Grass Flora. Available: http://www.kew.org/data/grasses-db.html.

DAI, Y., VAN SPRONSEN, J., WITKAMP, G., VERPOORTE, R. and CHOI, Y.H., 2013. *Natural deep eutectic solvents as new potential media for green technology.*

DE GAETANO, Y., MOHAMADOU, A., BOUDESOCQUE, S., HUBERT, J., PLANTIER-ROYON, R. and DUPONT, L., 2015. Ionic liquids derived from esters of Glycine Betaine: Synthesis and characterization. *Journal of Molecular Liquids,* **207**, pp. 60-66.

DEL RÍO, J.C., LINO, A.G., COLODETTE, J.L., LIMA, C.F., GUTIÉRREZ, A., MARTÍNEZ, ÁT., LU, F., RALPH, J. and RENCORET, J., 2015. Differences in the chemical structure of the lignins from sugarcane bagasse and straw. *Biomass and Bioenergy,* **81**, pp. 322-338.

DONGRE, P., DRISCOLL, M., AMIDON, T. and BUJANOVIC, B., 2015. Lignin-Furfural Based Adhesives. *Energies,* **8**(8), pp. 7897-7914.

DU, C., ZHAO, B., CHEN, X., BIRBILIS, N. and YANG, H., 2016. Effect of water presence on choline chloride-2urea ionic liquid and coating platings from the hydrated ionic liquid. *Scientific reports,* **6**.

FLORINDO, C., OLIVEIRA, F.S., REBELO, L.P.N., FERNANDES, A.M. and MARRUCHO, I.M., 2014. Insights into the Synthesis and Properties of Deep Eutectic Solvents Based on Cholinium Chloride and Carboxylic Acids. *ACS Sustainable Chemistry & Engineering,* **2**(10), pp. 2416-2425.

FRANCISCO, M., VAN DEN BRUINHORST, A. and KROON, M.C., 2013. Low-Transition-Temperature Mixtures (LTTMs): A New Generation of Designer Solvents. *Angewandte Chemie International Edition,* **52**(11), pp. 3074-3085.

FRANCISCO, M., VAN DEN BRUINHORST, A. and KROON, M.C., 2012. New natural and renewable low transition temperature mixtures (LTTMs): screening as solvents for lignocellulosic biomass processing. **14**(8), pp. 2153-2157.

FRANCISCO, M., VAN DEN BRUINHORST, A., ZUBEIR, L.F., PETERS, C.J. and KROON, M.C., 2013. A new low transition temperature mixture (LTTM) formed by choline chloride+lactic acid: Characterization as solvent for CO2 capture. *Fluid Phase Equilibria,* **340**, pp. 77-84.

GHAFFAR, S.H. and FAN, M., 2013. Structural analysis for lignin characteristics in biomass straw. *Biomass and Bioenergy,* **57**(Supplement C), pp. 264-279.

GHATEE, M.H., ZARE, M., MOOSAVI, F. and ZOLGHADR, A.R., 2010. Temperature-Dependent Density and Viscosity of the Ionic Liquids 1-Alkyl-3-methylimidazolium Iodides: Experiment and Molecular Dynamics Simulation. *Journal of Chemical & Engineering Data,* **55**(9), pp. 3084-3088.

GLASSER, W.G., BARNETT, C.A., MULLER, P.C. and SARKANEN, K.V., 1983. The chemistry of several novel bioconversion lignins. *Journal of Agricultural and Food Chemistry,* **31**(5), pp. 921-930.

GLASSER, W.G., DAVÉ, V. and FRAZIER, C.E., 1993. Molecular Weight Distribution of (Semi-) Commercial Lignin Derivatives. *Journal of Wood Chemistry and Technology,* **13**(4), pp. 545-559.

GORKE, J.T., SRIENC, F. and KAZLAUSKAS, R.J., 2008. Hydrolase-catalyzed biotransformations in deep eutectic solvents. *Chemical communications (Cambridge, England),* (10), pp. 1235.

GUERRA, A., FILPPONEN, I., LUCIA, L.A. and ARGYROPOULOS, D.S., 2006. Comparative evaluation of three lignin isolation protocols for various wood species. *Journal of agricultural and food chemistry,* **54**(26), pp. 9696-9705.

GUERRA, A., FILPPONEN, I., LUCIA, L.A., SAQUING, C., BAUMBERGER, S. and ARGYROPOULOS, D.S., 2006. Toward a better understanding of the lignin isolation process from wood. *Journal of agricultural and food chemistry,* **54**(16), pp. 5939-5947.

GUERRA, A., GASPAR, A.R., CONTRERAS, S., LUCIA, L.A., CRESTINI, C. and ARGYROPOULOS, D.S., 2007. On the propensity of lignin to associate: A size exclusion chromatography study with lignin derivatives isolated from different plant species. *Phytochemistry,* **68**(20), pp. 2570-2583.

HAGHBAKHSH, R. and RAEISSI, S., 2018. Densities and volumetric properties of (choline chloride + urea) deep eutectic solvent and methanol mixtures in the temperature range of 293.15–323.15 K. *The Journal of Chemical Thermodynamics,* **124**, pp. 10-20.

HAMMOND, O.S., BOWRON, D.T. and EDLER, K.J., 2017. The Effect of Water upon Deep Eutectic Solvent Nanostructure: An Unusual Transition from Ionic Mixture to Aqueous Solution. *Angewandte Chemie International Edition,* **56**(33), pp. 9782-9785.

HAMMOND, O.S., BOWRON, D.T. and EDLER, K.J., 2016. Liquid structure of the choline chloride-urea deep eutectic solvent (reline) from neutron diffraction and atomistic modelling. *Green Chemistry,* **18**(9), pp. 2736-2744.

HAN, M., KIM, Y., KOO, B. and CHOI, G., 2011. Bioethanol production by Miscanthus as a lignocellulosic biomass: Focus on high efficiency conversion to glucose and ethanol. *BioResources,* **6**(2),.

HERRERA, A., TÉLLEZ-LUIS, S.J., RAMÍREZ, J.A. and VÁZQUEZ, M., 2003. Production of Xylose from Sorghum Straw Using Hydrochloric Acid. *Journal of Cereal Science,* **37**(3), pp. 267-274.

ISIKGOR, F.H. and BECER, C.R., 2015. Lignocellulosic biomass: a sustainable platform for the production of bio-based chemicals and polymers. *Polym. Chem,* **6**(25), pp. 4497-4559.

JABLONSKÝ, M., KOČIŠ, J., HÁZ, A. and ŠIMA, J., 2015. Characterization and comparison by UV spectroscopy of precipitated lignins and commercial lignosulfonates. *Cellulose Chemistry and Technology,* **49**, pp. 267-274.

KARINEN, R., VILONEN, K. and NIEMELÄ, M., 2011. Biorefining: Heterogeneously Catalyzed Reactions of Carbohydrates for the Production of Furfural and Hydroxymethylfurfural. *ChemSusChem,* **4**(8), pp. 1002-1016.

KICK, M., KEIL, P. and KÖNIG, A., 2013. Solid–liquid phase diagram of the two Ionic Liquids EMIMCl and BMIMCl. *Fluid Phase Equilibria,* **338**, pp. 172-178.

KINDERMANN, G., MCCALLUM, I., FRITZ, S. and OBERSTEINER, M., 2008. A global forest growing stock, biomass and carbon map based on FAO statistics. *Silva Fennica,* **42**(3),.

KULP, K., 2000. *Handbook of Cereal Science and Technology, Revised and Expanded.* 2 edn. CRC Press.

KUMAR, A. and SHARMA, S., 2017. Recent updates on different methods of pretreatment of lignocellulosic feedstocks: a review. *Bioresources and Bioprocessing,* **4**(1), pp. 1-19.

LAZZÚS, J.A., 2012. A group contribution method to predict the melting point of ionic liquids. *Fluid Phase Equilibria,* **313**, pp. 1-6.

LOOW, Y., NEW, E.K., YANG, G.H., ANG, L.Y., FOO, L.Y.W. and WU, T.Y., 2017. Potential use of deep eutectic solvents to facilitate lignocellulosic biomass utilization and conversion. *Cellulose,* **24**(9), pp. 3591-3618.

LYNAM, J.G., KUMAR, N. and WONG, M.J., 2017. Deep eutectic solvents' ability to solubilize lignin, cellulose, and hemicellulose; thermal stability; and density. *Bioresource Technology,* **238**, pp. 684-689.

MENG, X., BALLERAT-BUSSEROLLES, K., HUSSON, P. and ANDANSON, J., 2016. Impact of water on the melting temperature of urea + choline chloride deep eutectic solvent. *New Journal of Chemistry,* **40**(5), pp. 4492-4499.

MOHAPATRA, S., MISHRA, C., BEHERA, S.S. and THATOI, H., 2017. Application of pretreatment, fermentation and molecular techniques for enhancing bioethanol production from grass biomass – A review. *Renewable and Sustainable Energy Reviews,* **78**(Supplement C), pp. 1007-1032.

PAUL, B.K., MOULIK, S.P. and KUNZ, W., 2015. *Ionic Liquid-Based Surfactant Science.* 1 edn. New York: John Wiley & Sons Inc.

PROCENTESE, A., JOHNSON, E., ORR, V., GARRUTO CAMPANILE, A., WOOD, J.A., MARZOCCHELLA, A. and REHMANN, L., 2015. Deep eutectic solvent pretreatment and subsequent saccharification of corncob. *Bioresource Technology,* **192**, pp. 31-36.

RENEWABLE FUELS ASSOCIATION, 2018-last update, Industry Statistics. Available: http://www.ethanolrfa.org/resources/industry/statistics/ [Apr 29, 2018].

RENGSTL, D., FISCHER, V. and KUNZ, W., 2014. Low-melting mixtures based on choline ionic liquids. *Physical Chemistry Chemical Physics,* **16**(41), pp. 22815-22822.

RUSS, C. and KÖNIG, B., 2012. Low melting mixtures in organic synthesis – an alternative to ionic liquids? *Green Chemistry,* **14**(11), pp. 2969.

SAAKE, B. and LEHNEN, R., 2007. Lignin. *Ullmann's Encyclopedia of Industrial Chemistry.*

SAMENI, J., KRIGSTIN, S. and SAIN, M., 2017. Solubility of Lignin and Acetylated Lignin in Organic Solvents. *BioResources,* **12**(1),.

SJÖSTRÖM, E., 1989. *Puukemia: teoreettiset perusteet ja sovellutukset.* 4. tark. p. edn. Espoo: Otakustantamo.

SMITH, E.L., ABBOTT, A.P. and RYDER, K.S., 2014. Deep Eutectic Solvents (DESs) and Their Applications. *Chemical reviews,* **114**(21), pp. 11060-11082.

STENIUS, P., 2000. *Forest Products Chemistry.* Finnish Paper Engineers' Association and TAPPI.

SUN, X., SUN, R., FOWLER, P. and BAIRD, M.S., 2005. Extraction and characterization of original lignin and hemicelluloses from wheat straw. *Journal of agricultural and food chemistry,* **53**(4), pp. 860-870.

TOLBERT, A., AKINOSHO, H., KHUNSUPAT, R., NASKAR, A.K. and RAGAUSKAS, A.J., 2014. Characterization and analysis of the molecular weight of lignin for biorefining studies. *Biofuels, Bioproducts and Biorefining,* **8**(6), pp. 836-856.

WANG, K., BAUER, S. and SUN, R., 2012. Structural Transformation of Miscanthus × giganteus Lignin Fractionated under Mild Formosolv, Basic Organosolv, and Cellulolytic Enzyme Conditions. *Journal of agricultural and food chemistry,* **60**(1), pp. 144-152.

WASSERSCHEID, P. and WELTON, T., 2008. *Ionic Liquids in Synthesis.* 2. edn. Weinheim: Wiley-VCH.

YIZHAK, M., 2018. The Entropy of Deep Eutectic Solvent Formation. *Entropy,* **20**(7),.

YOO, C.G., PU, Y. and RAGAUSKAS, A.J., 2017. Ionic liquids: Promising green solvents for lignocellulosic biomass utilization. *Current Opinion in Green and Sustainable Chemistry,* **5**(Supplement C), pp. 5-11.

ZENG, C., QI, S., XIN, R., YANG, B. and WANG, Y., 2016. Synergistic behavior of betaine–urea mixture: Formation of deep eutectic solvent. *Journal of Molecular Liquids,* **219**, pp. 74-78.

ZENG, J., HELMS, G.L., GAO, X. and CHEN, S., 2013. Quantification of wheat straw lignin structure by comprehensive NMR analysis. *Journal of agricultural and food chemistry,* **61**(46), pp. 10848-10857.

ZHEKENOV, T., TOKSANBAYEV, N., KAZAKBAYEVA, Z., SHAH, D. and MJALLI, F.S., 2017. Formation of type III Deep Eutectic Solvents and effect of water on their intermolecular interactions. *Fluid Phase Equilibria,* **441**, pp. 43-48.